PHYSICAL REVIEW D **82,** 083002 (2010)

Cosmic microwave background with Brans-Dicke gravity. I. Covariant formulation

Feng-Quan Wu,* Li-e Qiang, Xin Wang, and Xuelei Chen†

National Astronomical Observatories, Chinese Academy of Sciences, 20A Datun Road, Chaoyang District, Beijing 100012, China

(Received 23 December 2009; published 13 October 2010)

In the covariant cosmological perturbation theory, a 1 + 3 decomposition ensures that all variables in the frame-independent equations are covariant and gauge invariant and that they have clear physical interpretations. We develop this formalism in the case of Brans-Dicke gravity, and apply this method to the calculation of CMB anisotropy and large scale structures. We modify the publicly available Boltzmann code CAMB to calculate numerically the evolution of the background and adiabatic perturbations, and obtain the temperature and polarization spectra of Brans-Dicke theory for both scalar and tensor modes; the tensor mode results for Brans-Dicke gravity are obtained numerically for the first time. We first present our theoretical formalism in detail, and then explicitly describe the techniques used in modifying the CAMB code. These techniques are also very useful for other gravity models. Next we compare the CMB and large scale structure spectra in Brans-Dicke theory with those in the standard general relativity theory. At last, we investigate the integrated Sachs-Wolfe effect and the CMB lensing effect in Brans-Dicke theory. Constraints on the Brans-Dicke model with current observational data are presented in a companion paper [F. Wu and X. Chen, following Article, Phys. Rev. D **82**, 083003 (2010)] (paper II).

DOI: 10.1103/PhysRevD.82.083002 PACS numbers: 98.70.Vc, 04.50.Kd, 98.65.Dx

I. INTRODUCTION

The Jordan-Fierz-Brans-Dicke theory [1–5] (hereafter Brans-Dicke theory for simplicity) is a natural alternative and a simple generalization of Einstein's general relativity theory; it is also the simplest example of a scalar-tensor theory of gravity [6–10]. In Brans-Dicke theory, the purely metric coupling of matter with gravity is preserved, thus ensuring the universality of free fall (equivalence principle) and the constancy of all nongravitational constants. From early on, testing Brans-Dicke theory with CMB anisotropy has been considered [11]. However, the usual approach is to use a metric-based and gauge-dependent method, i.e. making the calculation with a particular gauge; see, e.g., Refs. [12–16].

The covariant approach to general relativity (GR) is an elegant solution to the ''gauge problem'' which has plagued the study of linear perturbation in gauge-dependent methods since the pioneering work of Lifshitz [17]. Before this problem was recognized, contradictory predictions of the behavior of perturbation of Friedmann-Lemaître-Robertson-Walker (FLRW) cosmologies were made. In 1980, Bardeen reformulated the metric approach using gauge-invariant variables [18] (see also Ref. [19] for a review on the variables, which has been widely used in recent perturbation calculations). However, as pointed out by Ellis [20], although the Bardeen variables are related to the density perturbations, they are not those perturbations themselves, since they include Fourier components of the metric tensor and other quantities in cunning combinations. The physical meaning of Bardeen's gauge-invariant variables is not always transparent. As emphasized by Hawking [21], the metric tensor cannot be measured directly, so it is not surprising that the variables used in the metric-based method do not always have a clear physical interpretation.

The covariant approach to general relativity and cosmology has its origins in the work of Heckmann, Schücking, Raychaudhuri, and Hawking [21–23]. In 1989, Ellis and Bruni proposed using the spatial gradient of matter density ($D_a\rho$) as the basic variable to describe density perturbations [20]. Subsequently, the cosmological applications have been developed extensively by Ellis and others in recent years [24–40]. The method has also been applied to problems in CMB physics [41–44]. Instead of using the components of the metric as basic variables, the covariant formalism performs a 1 + 3 split of the Bianchi and Ricci identities, using the kinematic quantities, energy-momentum tensors of the fluid(s), and the gravito-electromagnetic parts of the Weyl tensor to study how perturbations evolve. The most notable advantage of this method is that the covariant variables have transparent physical definitions, which ensures that predictions are always straightforward to interpret physically. Other advantages include the unified treatment of scalar, vector, and tensor modes; a systematic linearization procedure which can be extended to consider higher-order effects (this means the covariant variables are exactly gauge invariant, independent of any perturbative expansion); and the ability to linearize about a variety of background models, e.g. either the FLRW or the Bianchi models [45,46].

A pioneering work in applying the covariant approach to Brans-Dicke theory is Ref. [47], in which a conformal transformation was performed and the calculation was done in the Einstein frame. More recently, Refs. [48,49]

*wufq@bao.ac.cn
†xuelei@cosmology.bao.ac.cn

chose the effective fluid frame, implying $D_a\phi = 0$ and $\omega_{ab} = 0$; i.e. their foliation selects vorticity-free spacelike hypersurfaces in which $\phi = \text{const}$, and hence greatly simplifies the calculations.

The aim of this paper is to construct a full set of covariant and gauge-invariant linearized equations to calculate angular power spectra of CMB temperature and polarization anisotropies in the cold dark matter (CDM) frame, and to show that the covariant method will lead to a clear, mathematically well-defined description of the evolution of density perturbations. In a companion paper [50] (hereafter denoted paper II), we shall apply the formalism developed in this paper to the latest CMB and large scale structure data to obtain constraints on the Brans-Dicke parameter.

In Sec. II, we briefly review Brans-Dicke theory and its background cosmological evolution. The formalism of covariant perturbation theory is presented in Sec. III and the numerical implementation in Sec. IV. We discuss the results on primary anisotropy in Sec. V. The integrated Sachs-Wolfe (ISW) effect and gravitational lensing are discussed in Sec. VI. Finally, we summarize and conclude in Sec. VII.

Throughout this paper we adopt the metric signature $(+---)$. Our conventions for the Riemann and Ricci tensors are fixed by $[\nabla_a, \nabla_b]u_c = R_{abcd}u^d$, where ∇_a denotes the usual covariant derivative, and $R_{ab} \equiv R_{acb}{}^c$. We use ∂_a to represent an ordinary derivative. The spatially projected part of the covariant derivative is denoted by D_a. The index notation A_l denotes the index string $a_1 \ldots a_l$. Round brackets around indices denote symmetrization on the indices enclosed, square brackets denote antisymmetrization, and angled brackets denote the projected symmetric and trace-free (PSTF) parts. We adopt $\kappa = 8\pi G$ and use units with $\hbar = c = k_B = 1$ throughout. In the numerical work we use Mpc as units for distance.

II. BRANS-DICKE THEORY AND BACKGROUND COSMOLOGY

Brans-Dicke theory is a prototype of the scalar-tensor theory of gravity. One of its original motivations is to realize Mach's principle of inertia [4,5]. It introduced a new degree of freedom of the gravitational interaction in the form of a scalar field nonminimally coupled to the geometry. The action for Brans-Dicke theory in the usual (Jordan) frame is

$$\mathcal{S} = \frac{1}{16\pi}\int d^4x\sqrt{-g}\left[-\phi R + \frac{\omega}{\phi}g^{\mu\nu}\nabla_\mu\phi\nabla_\nu\phi\right] + \mathcal{S}^{(m)}, \tag{1}$$

where ϕ is the Brans-Dicke field, ω is a dimensionless parameter, and $\mathcal{S}^{(m)}$ is the action for the ordinary matter fields $\mathcal{S}^{(m)} = \int d^4x\sqrt{-g}\mathcal{L}^{(m)}$. Matter is not directly coupled to ϕ, in the sense that the Lagrangian density $\mathcal{L}^{(m)}$ does not depend on ϕ. For convenience, we also define a dimensionless field

$$\varphi = G\phi, \tag{2}$$

where G is the Newtonian gravitational constant measured today. The Einstein field equations are then generalized to

$$G_{\mu\nu} = \frac{8\pi G}{\varphi}T^{(m)}_{\mu\nu} + \frac{\omega}{\varphi^2}\left(\nabla_\mu\varphi\nabla_\nu\varphi - \frac{1}{2}g_{\mu\nu}\nabla_\lambda\varphi\nabla^\lambda\varphi\right) + \frac{1}{\varphi}(\nabla_\mu\nabla_\nu\varphi - g_{\mu\nu}\nabla_\lambda\nabla^\lambda\varphi), \tag{3}$$

where $T^{(m)}_{\mu\nu}$ is the stress tensor for all other matter except for the Brans-Dicke field, and it satisfies the energy-momentum conservation equation, $\nabla^\mu T^{(m)}_{\mu\nu} = 0$. The equation of motion for φ is

$$\nabla_a\nabla^a\varphi = \frac{\kappa}{2\omega + 3}T^{(m)}. \tag{4}$$

Here $T^{(m)} = T^{(m)\mu}_{\mu}$ is the trace of the energy-momentum tensor. The action (1) and the field equation (3) suggest that the Brans-Dicke field ϕ plays the role of the inverse of the gravitational coupling, $G_{\text{eff}}(\varphi) = \frac{1}{\phi} = \frac{G}{\varphi}$, which becomes a function of the space-time point.

For background cosmology, we treat ordinary matter as a perfect fluid with energy density ρ and pressure P,

$$T^{(m)}_{\mu\nu} = (\rho + P)u_\mu u_\nu - Pg_{\mu\nu}. \tag{5}$$

The equations describing the background evolution are

$$\rho' + 3\mathcal{H}(\rho + P) = 0, \tag{6}$$

$$\mathcal{H}^2 = \frac{\kappa S^2}{3\varphi}\rho + \frac{\omega}{6}\left(\frac{\varphi'}{\varphi}\right)^2 - \mathcal{H}\frac{\varphi'}{\varphi}, \tag{7}$$

$$\varphi'' + 2\mathcal{H}\varphi' = \frac{\kappa S^2}{2\omega + 3}(\rho - 3P), \tag{8}$$

where the prime denotes the derivative with respect to conformal time η, S is the scale factor, and $\mathcal{H} = S'/S$. General relativity is recovered in the limits

$$\omega \to \infty, \qquad \varphi' \to 0, \qquad \varphi'' \to 0. \tag{9}$$

To recover the value of Newton's gravitational constant today, which is determined by Cavendish-type experiments, we also require that the present-day value of φ be given by

$$\varphi_0 = \frac{2\omega + 4}{2\omega + 3}. \tag{10}$$

III. PERTURBATION THEORY

A. The 1 + 3 covariant decomposition

The main idea of the 1 + 3 decomposition is to make space-time splits of physical quantities with respect to the four-velocity u^a of an observer. There are many possible choices for the frame, for example, the CMB frame in which the dipole of CMB anisotropy vanishes, or the local

rest frame of matter. These frames are generally assumed to coincide when averaged on a sufficiently large scale. Here it will be convenient to choose u^a to coincide with the velocity of the CDM component, since u^a is then geodesic, and acceleration vanishes. From the four-velocity u^a, we could construct a projection tensor h_{ab} into the space perpendicular to u^a (the instantaneous rest space of observers whose four-velocity is u^a):

$$h_{ab} \equiv g_{ab} - u_a u_b, \tag{11}$$

where g_{ab} is the metric of the space-time. Since h_{ab} is a projection tensor, it can be used to obtain a covariant tensor perpendicular to u^a, and it satisfies

$$h_{ab} = h_{(ab)}, \qquad u^a h_{ab} = 0, \qquad h^c_a h_{cb} = h_{ab}, \qquad h^a_a = 3. \tag{12}$$

With the timelike four-velocity u_a and its tensor counterpart h_{ab}, one can decompose a space-time quantity into irreducible timelike and spacelike parts. For example, we can use u_a to define the covariant time derivatives of a tensor $T^{b\ldots c}{}_{d\ldots e}$:

$$\dot{T}^{b\ldots c}_{d\ldots e} \equiv u^a \nabla_a T^{b\ldots c}_{d\ldots e}. \tag{13}$$

Furthermore, we can exploit the projection tensor h_{ab} to define a spatial covariant derivative D^a which returns a tensor that is orthogonal to u^a on every index:

$$D^a T^{b\ldots c}{}_{d\ldots e} \equiv h^a_p h^b_r \ldots h^c_s h^t_d \ldots h^u_e \nabla^p T^{r\ldots s}{}_{t\ldots u}. \tag{14}$$

If the velocity field u^a has vanishing vorticity, D^a reduces to the covariant derivative in the hypersurfaces orthogonal to u^a. The PSTF parts of the vectors and rank-2 tensors are

$$V_{\langle a\rangle} = h_a{}^b V_b, \tag{15}$$

$$T_{\langle ab\rangle} = h_{\langle a}{}^c h_{b\rangle}{}^d T_{cd} = h_{(a}{}^c h_{b)}{}^d T_{cd} - \tfrac{1}{3} h^{cd} T_{cd} h_{ab}. \tag{16}$$

One can also define a volume element for the observer's instantaneous rest space:

$$\varepsilon_{abc} = \eta_{abcd} u^d = \varepsilon_{[abc]}, \tag{17}$$

where η_{abcd} is the four-dimensional volume element ($\eta_{abcd} = \eta_{[abcd]}$, $\eta_{0123} = -\sqrt{|g|}$). Note that $D_c h_{ab} = 0 = D_a \varepsilon_{bcd}$. The skew part of a projected rank-2 tensor is spatially dual to the projected vector $T_a = \frac{1}{2}\varepsilon_{abc} T^{[bc]}$, and any projected second-rank tensor has the irreducible covariant decomposition

$$T_{ab} = \tfrac{1}{3} T h_{ab} + \varepsilon_{abc} T^c + T_{\langle ab\rangle}, \tag{18}$$

where $T = T_{cd} h^{cd}$ is the spatial trace. In the 1 + 3 covariant formalism, all quantities are either scalars, projected vectors, or PSTF tensors. The covariant decompositions of the velocity gradient are

$$\nabla_a u_b = D_a u_b + u_a A_b, \tag{19}$$

$$D_a u_b = \omega_{ab} + \sigma_{ab} + \tfrac{1}{3}\theta h_{ab}, \tag{20}$$

where $\sigma_{ab} = \mathrm{D}_{\langle a} u_{b\rangle}$ is the shear tensor, which satisfies $\sigma_{ab} = \sigma_{(ab)}$, $\sigma^a_a = 0$, and $u^a \sigma_{ab} = 0$; $\omega_{ab} = \mathrm{D}_{[a} u_{b]}$ is the vorticity tensor, which satisfies $\omega_{ab} = \omega_{[ab]}$ and $u^a \omega_{ab} = 0$. One can also define the vorticity vector $\omega_a = \varepsilon_{abc}\omega^{bc}/2$ (with $\omega_{ab} = \varepsilon_{abc}\omega^c$). The scalar $\theta \equiv \nabla^a u_a = D^a u_a = 3H$ is the volume expansion rate, H is the local Hubble parameter, and $A_a \equiv u^b \nabla_b u_a = \dot{u}_a$ is the acceleration, which satisfies $u^a A_a = 0$. We note that the tensor $D_a u_b$ describes the relative motion of neighboring observers. The volume scalar θ determines the average separation between two neighboring observers. The effect of the vorticity is to change the orientation of a given fluid element without modifying its volume or shape; therefore it describes the rotation of matter flow. Finally, the shear describes the distortion of matter flow; it changes the shape while leaving the volume unaffected [35].

Gauge-invariant quantities can be constructed from scalar variables by taking their projected gradients. The comoving fractional projected gradient of the density field $\rho^{(i)}$ of a species i is the key quantity of the covariant method [20],

$$X^{(i)}_a \equiv \frac{S}{\rho^{(i)}} D_a \rho^{(i)}, \tag{21}$$

which describes the density variation between two neighboring fundamental observers. The comoving spatial gradient of the expansion rate orthogonal to the fluid flow is

$$Z_a \equiv S D_a \theta, \tag{22}$$

which describes perturbations in the expansion. These quantities are, in principle, observable, characterizing inhomogeneity in a covariant way, and they vanish in the FLRW limit.

The matter stress-energy tensor $T^{(m)}_{ab}$ can be decomposed irreducibly with respect to u^a as follows:

$$T^{(m)}_{ab} \equiv \rho u_a u_b + 2u_{(a} q_{b)} - P h_{ab} + \pi_{ab}, \tag{23}$$

where $\rho \equiv T^{(m)}_{ab} u^a u^b$ is the density of matter measured by an observer moving with four-velocity u^a, $q_a \equiv h^b_a T^{(m)}_{bc} u^c$ is the relativistic momentum density or heat (i.e. energy) flux and is orthogonal to u^a, $P \equiv -h^{ab} T^{(m)}_{ab}/3$ is the isotropic pressure, and the projected symmetric traceless tensor $\pi_{ab} \equiv T^{(m)}_{\langle ab\rangle}$ is the anisotropic stress, which is also orthogonal to u^a. The quantities ρ, P, q_a, π_{ab} are referred to as *dynamical quantities* and σ_{ab}, ω_{ab}, θ, A_a as *kinematical quantities*. In the FLRW limit, isotropy restricts $T^{(m)}_{ab}$ to the perfect-fluid form, so the heat flux q_a and anisotropic stress π_{ab} must vanish.

The remaining first-order gauge-invariant variables that we need are derived from the Weyl tensor C_{abcd}, which is associated with the long-range gravitational field and vanishes in an exact FLRW universe due to isotropy.

In analogy to the electromagnetic field, the Weyl tensor can be split into electric and magnetic parts, denoted by E_{ab} and B_{ab}, respectively. They are both symmetric traceless tensors and are orthogonal to u^a,

$$E_{ab} \equiv C_{acbd}u^c u^d = E_{\langle ab\rangle}, \tag{24}$$

$$B_{ab} \equiv -{}^*C_{acbd}u^c u^d = -\tfrac{1}{2}\varepsilon_a{}^{ef}C_{efbd}u^d = B_{\langle ab\rangle}. \tag{25}$$

Here $*$ denotes the dual, ${}^*C_{acbd} = \frac{1}{2}\eta_{ac}{}^{ef}C_{efbd}$.

For the radiation field, we can make a 1 + 3 covariant decomposition of the photon four-momentum as

$$p^a = E(u^a + e^a), \tag{26}$$

where $E = p^a u_a$ is the energy of the photon. e^a describes the propagation direction of the photon in the instantaneous rest space of the observer. The observer can introduce a pair of orthogonal polarization vectors $(e_1)^a$ and $(e_2)^a$, which are perpendicular to u^a and e^a, to form a right-handed orthonormal tetrad $\{u^a, (e_1)^a, (e_2)^a, e^a\}$ at the observation point. The (screen) projection tensor is defined as

$$\mathcal{H}_{ab} = g_{ab} - u_a u_b + e_a e_b, \tag{27}$$

which is perpendicular to both u^a and e^a, and satisfies $\mathcal{H}^a_b(e_1)^b = (e_1)^a$.

Using the polarization basis vectors, the observer can decompose an arbitrary radiation field into Stokes parameters $I(E, e^a)$, $Q(E, e^a)$, $U(E, e^a)$, and $V(E, e^a)$ [41]. Therefore one can introduce a second-rank transverse polarization tensor $P_{ab}(E, e^c)$,

$$P_{ab}(e_i)^a(e_j)^b = \frac{1}{2}\begin{pmatrix} I+Q & U+V \\ U-V & I-Q \end{pmatrix}, \tag{28}$$

for i and $j = 1, 2$, and we have omitted the arguments E and e^a. $P_{ab} \propto E^3\mathcal{H}^c_a\mathcal{H}^d_b f_{cd}$, where f_{cd} is a photon distribution function. Decomposing $P_{ab}(E, e^d)$ into its irreducible components, one obtains

$$P_{ab}(E, e^d) = -\tfrac{1}{2}I(E, e^d)\mathcal{H}_{ab} + \mathcal{P}_{ab}(E, e^d) + \tfrac{1}{2}V(E, e^d)\epsilon_{abc}e^c, \tag{29}$$

where the linear polarization tensor $\mathcal{P}_{ab}(E, e^d)$ satisfies

$$\mathcal{P}_{ab}(e_i)^a(e_j)^b = \frac{1}{2}\begin{pmatrix} Q & U \\ U & -Q \end{pmatrix}. \tag{30}$$

It is convenient to define the energy-integrated multipole for the total intensity brightness and the electric part of the linear polarization:

$$I_{A_l} = \int_0^\infty \mathrm{d}E \int \mathrm{d}\Omega I(E, e^c)e_{\langle A_l\rangle}, \tag{31}$$

$$\mathcal{E}_{A_l} = M_l^2 \int_0^\infty \mathrm{d}E \int \mathrm{d}\Omega e_{\langle A_{l-2}}\mathcal{P}_{a_{l-1}a_l\rangle}(E, e^c), \tag{32}$$

where $e_{A_l} = e_a e_b e_c \ldots e_l$ and $M_l \equiv \sqrt{2l(l-1)/[(l+1)(l+2)]}$.

B. The linearized perturbation equations

In the 1 + 3 covariant approach, the fundamental quantities are not the metrics, which are gauge dependent, but the kinematic quantities of the fluid, namely, the shear σ_{ab}, the vorticity ω_{ab}, the volume expansion rate θ, the acceleration A_a, the energy-momentum of matter, and the gravito-electromagnetic parts of the Weyl tensor. The fundamental equations governing these quantities are the Bianchi identities and the Ricci identities. The Riemann tensor in these equations is expressed in terms of E_{ab}, B_{ab}, and the Ricci tensor R_{ab}. The modified Einstein equation connects the Ricci tensor to the matter energy-momentum tensor. In the following, we have linearized all the perturbation equations. We should also note that the definitions of the covariant variables do not assume any linearization, and exact equations can be found for their evolution.

The first set of equations is derived from the Ricci identities for the vector field u^a, i.e.

$$2\nabla_{[a}\nabla_{b]}u_c = R_{abcd}u^d. \tag{33}$$

Substituting the four-velocity gradient (19) and the decomposition of the Riemann tensor, and separating out the timelike projected part into the trace, the symmetric trace-free part, and the skew symmetric part, we obtain three propagation equations. The first propagation equation is the Raychaudhuri equation,

$$\dot\theta + \frac{1}{3}\theta^2 - D^a\dot u_a + \frac{\kappa}{2\varphi}(\rho + 3P) + \frac{1}{2}\left(2\omega\frac{\dot\varphi^2}{\varphi^2} + \frac{1}{\varphi}D_aD^a\varphi + \theta\frac{\dot\varphi}{\varphi} + 3\frac{\ddot\varphi}{\varphi}\right) = 0, \tag{34}$$

which is the key equation of gravitational collapse, accounting for the time evolution of θ. The second is the vorticity propagation equation,

$$\dot\omega_{ab} - D_{[a}\dot u_{b]} + \tfrac{2}{3}\theta\omega_{ab} = 0. \tag{35}$$

The last one is the shear propagation equation,

$$\dot\sigma_{\langle ab\rangle} + \frac{2}{3}\theta\sigma_{ab} - D_{\langle a}\dot u_{b\rangle} + E_{ab} + \frac{\kappa}{2}\frac{\pi_{ab}}{\varphi} + \frac{1}{2\varphi}D_{\langle b}D_{a\rangle}\varphi + \frac{1}{2}\frac{\dot\varphi}{\varphi}\sigma_{ab} = 0, \tag{36}$$

which describes the evolution of kinematical anisotropies. It shows that the tidal gravitational field E_{ab} and the anisotropic stress π_{ab} would induce the shear directly, and the shear will change the spatial inhomogeneity of the expansion through the constraint equations (37).

The propagation equations are complemented by three constraint equations, which are spacelike components of Eq. (33). The first is the shear constraint,

$$D^b\omega_{ab} + D^b\sigma_{ab} - \frac{2}{3}D_a\theta - \frac{\kappa}{\varphi}q_a - \omega\frac{\dot\varphi}{\varphi^2}D_a\varphi - \frac{1}{\varphi}(D_a\varphi)^{\cdot} - \frac{\dot\varphi}{\varphi}\dot u_a = 0, \tag{37}$$

which shows the relation between the momentum flux q_a, the shear σ_{ab}, and the spatial inhomogeneity of the expansion. The second constraint equation is the vorticity divergence identity,

$$D^c(\varepsilon_{abc}\omega^{ab}) = 0. \tag{38}$$

The last one is the B_{ab} equation,

$$B_{ab} + (D^c\omega_{d(a} + D^c\sigma_{d(a)})\eta^d_{b)ce}u^e = 0, \tag{39}$$

which shows that the magnetic Weyl tensor can be constructed from the vorticity tensor and the shear tensor. With this last equation B_{ab} may be eliminated from some equations in favor of the vorticity and the shear.

So far we have only discussed propagation and constraint equations for the kinematic quantities. The second set of equations arises from the Bianchi identities of the Riemann tensor,

$$\nabla_{[e}R_{cd]ab} = 0, \tag{40}$$

which gives a constraint on the curvature tensor and leads to the Bianchi identities for the Weyl tensor after contracting once,

$$\nabla^d C_{abcd} = \nabla_{[b}R_{a]c} + \tfrac{1}{6}g_{c[b}\nabla_{a]}R. \tag{41}$$

The 1 + 3 splitting of the once-contracted Bianchi identities leads to two propagation and two constraint equations which are similar in form to the Maxwell field equations in an expanding universe, governing the evolution of the long-range gravitational field. The first propagation equation is the $\dot{E}$ equation,

$$\begin{aligned}\dot{E}_{ab} &+ \theta E_{ab} + D^c B_{d(a}\eta_{b)ce}{}^d u^e + \frac{\kappa}{6\varphi}[3(\rho + P)\sigma_{ab} \\ &+ 3D_{\langle a}q_{b\rangle} - 3\dot{\pi}_{ab} - \theta\pi_{ab}] + \frac{1}{2}\sigma_{ab}\left(\omega + \frac{3}{2}\right)\frac{\dot{\varphi}^2}{\varphi^2} \\ &- \frac{1}{6}\frac{\sigma_{ab}}{\varphi}D_\mu D^\mu\varphi + \frac{1}{2}\left(\omega + \frac{3}{2}\right)\frac{\dot{\varphi}}{\varphi^2}D_{\langle a}D_{b\rangle}\varphi \\ &+ \frac{1}{2}\frac{\dot{\varphi}}{\varphi}E_{ab} + \frac{3}{4}\kappa\frac{\dot{\varphi}}{\varphi^2}\pi_{ab} = 0,\end{aligned} \tag{42}$$

and the second propagation equation is the $\dot{B}$ equation

$$\begin{aligned}\dot{B}_{ab} &+ \left(\theta + \frac{\dot{\varphi}}{2\varphi}\right)B_{ab} - \Big[D^c E_{d(a} + \frac{\kappa}{2\varphi}D^c\pi_{d(a} \\ &+ \frac{1}{2\varphi}D^c D_d D_{(a}\varphi - \frac{1}{6\varphi}D^c D_\mu D^\mu\varphi h_{d(a}\Big]\eta_{b)ce}{}^d u^e = 0.\end{aligned} \tag{43}$$

This pair of equations for electric and magnetic parts of the Weyl tensor would give rise to wavelike behavior for its propagation: if we take the time derivative of the $\dot{E}$ equation, commuting the time and spatial derivatives of the B term and substituting from the $\dot{B}$ equation to eliminate B, we would obtain an $\ddot{E}$ term and a double spatial derivatives term, which together give the wave operator acting on E; similarly we can obtain a wave equation for B by taking the time derivative of the $\dot{B}$ equation. These waves are also subjected to two constraint equations, which emerge from the spacelike component of the decomposed equation (41). The first constraint is

$$\begin{aligned}D^b E_{ab} &- \frac{\kappa}{6\varphi}(2D_a\rho + 2\theta q_a + 3D^b\pi_{ab}) + \frac{2\kappa}{3}\rho\frac{D_a\varphi}{\varphi^2} \\ &- \frac{\kappa}{2}\frac{\dot{\varphi}}{\varphi^2}q_a - \left(\frac{\omega}{3} + \frac{1}{2}\right)\frac{\dot{\varphi}}{\varphi^2}\left[\frac{4}{3}\theta D_a\varphi + (D_a\varphi)^{\cdot} + \dot{u}\,\dot{\varphi}\right] = 0.\end{aligned} \tag{44}$$

This is the div E equation, with the source term given by the spatial gradient of the energy density. It can be regarded as a vector analogue of the Newtonian Poisson equation, and it shows that the scalar modes will result in a nonzero divergence of E_{ab}, and hence a nonzero gravitational E field. The second constraint equation is

$$\begin{aligned}D^b B_{ab} &- \frac{\kappa}{2\varphi}[(\rho + P)\eta_{ab}{}^{cd}u^b\omega_{cd} + \eta_{abcd}u^b D^c q^d] \\ &- \frac{1}{2}\Big[\left(\omega\frac{\dot{\varphi}^2}{\varphi^2} - \frac{1}{3\varphi}D_\mu D^\mu\varphi - \frac{\theta}{3}\frac{\dot{\varphi}}{\varphi} + \frac{\ddot{\varphi}}{\varphi}\right)\eta_{ab}{}^{cd}u^b\omega_{cd} \\ &+ \eta_{abcd}u^b\Big(\omega\frac{\dot{\varphi}}{\varphi^2}D^c D^d\varphi + \frac{1}{\varphi}(D^c D^d\varphi)^{\cdot} + \frac{\theta}{3\varphi}D^c D^d\varphi \\ &+ \frac{\dot{\varphi}}{\varphi}D^c\dot{u}^d\Big)\Big] = 0.\end{aligned} \tag{45}$$

This is the div B equation, with the fluid vorticity serving as the source term. It shows that the vector modes will result in nonzero divergence of B_{ab}, and hence a nonzero gravitational B field. The above equations are remarkably similar to the Maxwell equations of the electromagnetism, so we have chosen to use E_{ab} and B_{ab} as the symbols.

The last set of equations arises from the twice-contracted Bianchi identities. Projecting parallel and orthogonal to u^a, we obtain two propagation equations,

$$\dot{\rho} + \theta(\rho + P) + D_a q^a = 0, \tag{46}$$

$$\dot{q}_a + \tfrac{4}{3}\theta q_a + (\rho + P)\dot{u}_a + D^b\pi_{ab} - D_a P = 0, \tag{47}$$

respectively. For perfect fluids, these reduce to

$$\dot{\rho} + \theta(\rho + P) = 0, \tag{48}$$

$$(\rho + P)\dot{u}_a - D_a P = 0, \tag{49}$$

which are the energy conservation equation and momentum conservation equation, respectively.

The background field equation for the Brans-Dicke field is given in Eq. (8). The first-order covariant and gauge-invariant perturbation variable of the Brans-Dicke field is defined as the spatial derivative of the Brans-Dicke field,

$$\mathcal{V}_a \equiv SD_a\varphi. \tag{50}$$

Taking the covariant spatial derivative of Eq. (8), and commuting the spatial and time derivatives of the $\mathcal{V}$ term, we could obtain the first-order perturbation equation for the Brans-Dicke field after linearization,

$$\mathcal{V}_a'' + 2\mathcal{H}\mathcal{V}_a' + SZ_a\varphi' + S^2 D_a D^b \mathcal{V}_b = \frac{\kappa S^2}{3+2\omega}\sum_i (1 - 3c_s^{(i)2})\rho^{(i)}X^{(i)}, \tag{51}$$

where the upper index (i) labels the particle species.

In the absence of rotation, $\omega_{ab} = 0$, one can define global three-dimensional spacelike hypersurfaces that are everywhere orthogonal to u^a. This three-surface is meshed by the instantaneous rest space of comoving observers. The geometry of the hypersurfaces is determined by the three-Riemann tensor defined by

$$[D_a, D_b]u_c = {}^{(3)}R_{abdc}u^d, \tag{52}$$

which is similar to the definition of the Riemann tensor R_{abdc} but with a conventional opposite sign. The relationship between ${}^{(3)}R_{abdc}$ and R_{abdc} is

$$\begin{aligned} {}^{(3)}R_{abcd} &= -h_a{}^q h_b{}^s h_c{}^f h_d{}^p R_{qsfp} - \upsilon_{ac}\upsilon_{bd} + \upsilon_{ad}\upsilon_{bc} \\ &= {}^{(3)}R_{[ab][cd]}, \end{aligned} \tag{53}$$

where $\upsilon_{ab} = \mathrm{D}_b u_a$ is the relative flow tensor between two neighboring observers. In analogy to four dimensions, the projected Ricci tensor and Ricci scalar are defined by

$${}^{(3)}R_{ab} = {}^{(3)}R_{acbd}h^{cd} = {}^{(3)}R^c{}_{acb} \tag{54}$$

and

$${}^{(3)}R = {}^{(3)}R_{ab}h^{ab}. \tag{55}$$

The ${}^{(3)}R_{ab}$ is determined by the Gauss-Codacci formula

$${}^{(3)}R_{ab} = \frac{1}{3}{}^{(3)}R h_{ab} - \frac{1}{3}\theta\sigma_{ab} - \frac{\kappa}{2}\pi_{ab} + E_{ab}, \tag{56}$$

where

$${}^{(3)}R = 2(\kappa\rho - \tfrac{1}{3}\theta^2). \tag{57}$$

Equation (57) is also the generalized Friedmann equation, showing how the matter tensor determines the three-space average curvature.

The last first-order covariant and gauge-invariant variables can be obtained from the spatial derivative of the projected Ricci scalar,

$$\eta_a \equiv \tfrac{1}{2}SD_a{}^{(3)}R. \tag{58}$$

After a tedious calculation, we obtain

$$\begin{aligned} \eta_a = {} & \kappa\frac{\rho X_a}{\varphi} - \kappa\frac{\rho\mathcal{V}_a}{\varphi^2} - \frac{1}{S}\left(2\mathcal{H} + \frac{\varphi'}{\varphi}\right)Z_a \\ & + \frac{1}{S^2}\left(\omega\frac{\varphi'}{\varphi^2} - \frac{3\mathcal{H}}{\varphi}\right)(\mathcal{V}_a' - \mathcal{H}\mathcal{V}_a) \\ & + (\omega+3)\frac{1}{S^2}\frac{\varphi'}{\varphi^2}\mathcal{H}\mathcal{V}_a + \frac{1}{S}\left(\omega\frac{\varphi'^2}{\varphi^2} - 3\mathcal{H}\frac{\varphi'}{\varphi}\right)W_a \\ & - \frac{\omega}{S^2}\frac{\varphi'^2}{\varphi^3}\mathcal{V}_a - \frac{1}{\varphi}D_a D_\nu \mathcal{V}^\nu - \frac{3}{S}\mathcal{H}^2\frac{\mathcal{V}_a}{\varphi}. \end{aligned} \tag{59}$$

C. Mode expansion in spherical harmonics

In the linear perturbation theory it is convenient to expand the $O(\epsilon)$ variables in harmonic modes, since it splits the perturbations into scalar, vector, or tensor modes and decouples the temporal and spatial dependencies of the 1 + 3 equations. This converts the constraint equations into algebraic relations and the propagation equations into ordinary differential equations along the flow lines. In this paper we focus on the scalar and tensor perturbation modes, since the vector modes would decay in an expanding universe in the absence of sources such as topological defects.

1. Scalar mode

For scalar perturbations we expand in the scalar eigenfunctions $Q^{(k)}$ of the generalized Helmholtz equation

$$S^2 D^a D_a Q^{(k)} = k^2 Q^{(k)} \tag{60}$$

at zero order. They are defined so as to be constant along flow lines, i.e. independent of the proper time $\dot{Q}^{(k)} = O(\epsilon)$, and orthogonal to the fluid four-velocity u^a.

For the lth multipoles of the radiation anisotropy and polarization, we expand in the rank-l PSTF tensor $Q^{(k)}_{A_l}$, derived from the scalar harmonics with

$$Q^{(k)}_{A_l} = \left(\frac{S}{k}\right)^l D_{\langle a_1 \ldots} D_{a_l\rangle} Q^{(k)}, \tag{61}$$

where the index notation A_l denotes the index string $a_1 \ldots a_l$. The recursion relation for $Q^{(k)}_{A_l}$,

$$Q^{(k)}_{A_l} = \frac{S}{k} D_{\langle a_l} Q^{(k)}_{A_{l-1}\rangle}, \tag{62}$$

follows directly from Eq. (61). The factor of $(S/k)^l$ in the definition of $Q^{(k)}_{A_l}$ ensures that $\dot{Q}^{(k)}_{A_l} = 0$ at zero order. $Q^{(k)}_{A_l}$ also satisfies some other zero-order properties,

$$u^{a_i} Q^{(k)}_{a_1..a_i..a_l} = 0, \qquad h^{a_i a_j} Q^{(k)}_{a_1..a_i..a_j..a_l} = 0. \tag{63}$$

We also have the following differential relations which can be derived from Eqs. (60) and (62):

$$D^{a_1} Q^{(k)}_{a_1 a_2 \ldots a_l} = \frac{l}{2l-1}\frac{k}{S}\left[1 - (l^2-1)\frac{K}{k^2}\right]Q^{(k)}_{a_2 \ldots a_l}, \tag{64}$$

$$D^2 Q^{(k)}_{a_1\ldots a_l} = \frac{k^2}{S^2}\left[1 - l(l+1)\frac{K}{k^2}\right] Q^{(k)}_{a_1\ldots a_l}. \quad (65)$$

Now we can expand the gauge-invariant variable in the following dimensionless harmonic coefficients:

$$X^{(i)}_a = \sum_k k X^{(i)}_k Q^{(k)}_a, \quad (66)$$

$$Z_a = \sum_k \frac{k^2}{S} Z_k Q^{(k)}_a, \quad (67)$$

$$q^{(i)}_a = \rho^{(i)} \sum_k q^{(i)}_k Q^{(k)}_a, \quad (68)$$

$$v^{(i)}_a = \sum_k v^{(i)}_k Q^{(k)}_a, \quad (69)$$

$$\pi^{(i)}_{ab} = \rho^{(i)} \sum_k \pi^{(i)}_k Q^{(k)}_{ab}, \quad (70)$$

$$E_{ab} = \sum_k \frac{k^2}{S^2} \Phi_k Q^{(k)}_{ab}, \quad (71)$$

$$\sigma_{ab} = \sum_k \frac{k}{S} \sigma_k Q^{(k)}_{ab}, \quad (72)$$

$$A_a = \sum_k \frac{k}{S} W_k Q^{(k)}_a, \quad (73)$$

$$\mathcal{V}_a = \sum_k k \mathcal{V}_k Q^{(k)}_a, \quad (74)$$

$$\eta_a = \sum_k \frac{k^3}{S^2} \eta_k Q^{(k)}_a, \quad (75)$$

$$I_{A_l} = \rho_\gamma \sum_k I^{(l)}_k Q^{(k)}_{A_l}, \quad (76)$$

$$\mathcal{E}_{A_l} = \rho_\gamma \sum_k \mathcal{E}^{(l)}_k Q^{(k)}_{A_l}, \quad (77)$$

where the upper index (i) labels the particle species. The scalar expansion coefficients, such as $X^{(i)}_a$, are first-order gauge-invariant variables, and their spatial gradients are second order, for example, $D^a X^{(i)}_k = O(2)$. In the covariant and gauge-invariant approach, we characterize scalar perturbations by requiring that the vorticity and the magnetic part of the Weyl tensor be at most second order. Demanding $\omega_{ab} = O(2)$ ensures that density gradients are not from kinematic effects due to vorticity, and setting $B_{ab} = O(2)$ ensures that gravitational waves are excluded from the first order.

To obtain the scalar equations for the scalar expansion coefficients, one could substitute the harmonic expansions of the covariant variables into the propagation and constraint equations given in the section above. Here we will consider only the adiabatic modes. For the (i) fluid,

$$D^a P^{(i)} = c_s^{(i)2} D^a \rho^{(i)}, \quad (78)$$

where $c_s^{(i)}$ is the adiabatic sound speed of the (i) fluid. For the spatial gradients of the total density X_k, we find

$$X_k' + \frac{3\mathcal{H}}{\rho}\sum_i \rho^{(i)} X^{(i)}_k \left(c_s^{(i)2} - \frac{P}{\rho}\right) + k\left[\left(1 + \frac{P}{\rho}\right) Z_k + \sum_i q^{(i)}_k\right] - 3\mathcal{H}\left(1 + \frac{P}{\rho}\right) W_k = 0. \quad (79)$$

For the individual fluid of the (i) species, the propagation equation satisfies

$$X_k'^{(i)} + 3\mathcal{H}\left(c_s^{(i)2} - \frac{P^{(i)}}{\rho^{(i)}}\right) X^{(i)}_k + k\left[\left(1 + \frac{P^{(i)}}{\rho^{(i)}}\right) Z_k + q^{(i)}_k\right] - 3\mathcal{H}\left(1 + \frac{P^{(i)}}{\rho^{(i)}}\right) W_k = 0. \quad (80)$$

For the heat fluxes, we have

$$q_k'^{(i)} + \mathcal{H}\left(1 - 3\frac{P^{(i)}}{\rho^{(i)}}\right) q^{(i)}_k + \left(1 + \frac{P^{(i)}}{\rho^{(i)}}\right) k W_k + \frac{2}{3} k \left(1 - \frac{3K}{k^2}\right) \pi^{(i)}_k - k c_s^{(i)2} X^{(i)}_k = 0. \quad (81)$$

The heat flux for each fluid component is often given by $q^{(i)}_k = (\rho^{(i)} + P^{(i)}) v^{(i)}_k$, so we can derive the propagation equations for $v^{(i)}_k$ from Eq. (81).

We also can obtain the time evolution of the spatial gradient of the expansion,

$$Z_k' + \mathcal{H} Z_k + \frac{W_k}{k}(3\mathcal{H}' - 3\mathcal{H}^2 - k^2) + \frac{1}{k}\frac{\kappa S^2}{2\varphi}\sum_i (1 + 3c_s^{(i)2})\rho^{(i)} X^{(i)}_k + \frac{1}{2k}\left\{\mathcal{V}_k\left[-4\omega\frac{\varphi'^2}{\varphi^3} - 3\frac{\varphi''}{\varphi^2} - \frac{S^2\kappa}{\varphi^2}(\rho + 3P) + \frac{k^2}{\varphi}\right] + 4\omega\frac{\varphi'}{\varphi^2}\mathcal{V}_k' + 3\frac{\mathcal{V}_k''}{\varphi} + k Z_k \frac{\varphi'}{\varphi} + W_k\left(4\omega\frac{\varphi'^2}{\varphi^2} + 6\frac{\varphi''}{\varphi} - 3\mathcal{H}\frac{\varphi'}{\varphi}\right) + 3\frac{\varphi'}{\varphi} W_k'\right\} = 0. \quad (82)$$

Substituting the covariant harmonic expansion into Eq. (59), and then taking the time derivative of this equation, we obtain the evolution of the spatial gradient of the three-curvature scalar:

$$k^2\eta_k' = -X_k\left[S^2\kappa(\rho+3P)\frac{\mathcal{H}}{\varphi}+S^2\kappa\rho\frac{\varphi'}{\varphi^2}\right]+S^2\kappa\rho\frac{X_k'}{\varphi}+\mathcal{V}_k\left[S^2\kappa(\rho+3P)\frac{\mathcal{H}}{\varphi^2}+\frac{3}{2}S^2\kappa(\rho-P)\frac{\varphi'}{\varphi^3}+3\mathcal{H}\frac{\varphi''}{\varphi^2}-6\frac{\varphi'^2}{\varphi^3}\mathcal{H}\right.$$
$$\left.-\left(2\omega+\frac{3}{2}\right)\frac{\varphi'\varphi''}{\varphi^3}+2\omega\frac{\varphi'^3}{\varphi^4}+k^2\frac{\varphi'}{\varphi^2}\right]+\mathcal{V}_k'\left[\frac{S^2\kappa}{2\varphi^2}(3P-\rho)+\left(\omega+\frac{3}{2}\right)\frac{\varphi''}{\varphi^2}-2\omega\frac{\varphi'^2}{\varphi^3}+6\mathcal{H}\frac{\varphi'}{\varphi^2}-\frac{k^2}{\varphi}\right]$$
$$+\mathcal{V}_k''\left(\omega\frac{\varphi'}{\varphi^2}-\frac{3\mathcal{H}}{\varphi}\right)+W_k\left(2\omega\frac{\varphi'\varphi''}{\varphi^2}-2\omega\frac{\varphi'^3}{\varphi^3}-3\mathcal{H}'\frac{\varphi'}{\varphi}-3\mathcal{H}\frac{\varphi''}{\varphi}+3\mathcal{H}\frac{\varphi'^2}{\varphi^2}\right)+W_k'\left(\omega\frac{\varphi'^2}{\varphi^2}-3\mathcal{H}\frac{\varphi'}{\varphi}\right)$$
$$-kZ_k\left(2\mathcal{H}'+\frac{\varphi''}{\varphi}-\frac{\varphi'^2}{\varphi^2}\right)-kZ_k'\left(2\mathcal{H}+\frac{\varphi'}{\varphi}\right). \tag{83}$$

As mentioned by Ref. [51], by solving the propagation equation of η_k, we avoid the numerical instability problem in isocurvature modes when we work in the CDM frame.

From the shear propagation equation (36), the propagation equation for σ_k becomes

$$\sigma_k'+\mathcal{H}\sigma_k-kW_k+k\Phi_k+\frac{S^2}{k}\frac{\kappa}{2\varphi}\rho\pi_k+k\frac{\mathcal{V}_k}{2\varphi}+\frac{1}{2}\frac{\varphi'}{\varphi}\sigma_k=0. \tag{84}$$

From the div E equation (44), we could obtain the Φ_k equation,

$$2\frac{k^3}{S^3}\left(1-3\frac{K}{k^2}\right)\Phi_k-\frac{k}{S}\frac{\kappa\rho}{\varphi}\left[X_k+\left(1-3\frac{K}{k^2}\right)\pi_k\right]-\frac{3\mathcal{H}}{S}\frac{\kappa\rho}{\varphi}q_k+2\frac{k}{S}\kappa\rho\frac{\mathcal{V}_k}{\varphi^2}-\frac{3}{2}\frac{1}{S}\frac{\varphi'}{\varphi^2}\kappa\rho q_k$$
$$-\left(\omega+\frac{3}{2}\right)\frac{k}{S^3}\frac{\varphi'}{\varphi^2}(\mathcal{V}_k'+3\mathcal{H}\mathcal{V}_k+W_k\varphi')=0. \tag{85}$$

The algebraic equation of σ_k can be derived from the shear constraint equation (37),

$$\frac{3}{2}k\left[Z_k-\sigma_k\left(1-3\frac{K}{k^2}\right)\right]+\frac{S^2}{k}\frac{\kappa}{\varphi}\rho q_k+\omega\frac{\varphi'}{\varphi^2}\mathcal{V}_k+\frac{1}{\varphi}(\mathcal{V}_k'-\mathcal{H}\mathcal{V}_k)+\frac{\varphi'}{\varphi}W_k=0. \tag{86}$$

From the first-order perturbation equation for the Brans-Dicke field (51), we could derive the quadratic differential equation of $\mathcal{V}_k$,

$$\mathcal{V}_k''+2\mathcal{H}\mathcal{V}_k'+kZ_k\varphi'+k^2\mathcal{V}_k=\frac{\kappa S^2}{3+2\omega}\sum_i(1-3c_s^{(i)2})\rho^{(i)}X^{(i)}. \tag{87}$$

The variables X_k, q_k, and π_k [without the upper index (i)] refer to variables of the total matter, and can be expressed as

$$\rho X_k=\rho^{(\gamma)}X_k^{(\gamma)}+\rho^{(\nu)}X_k^{(\nu)}+\rho^{(b)}X_k^{(b)}+\rho^{(c)}X_k^{(c)}, \tag{88}$$

$$\rho q_k=\rho^{(\gamma)}q_k^{(\gamma)}+\rho^{(\nu)}q_k^{(\nu)}+(\rho^{(b)}+p^{(b)})v_k^{(b)}+\rho^{(c)}v_k^{(c)}, \tag{89}$$

$$\rho\pi_k=\rho^{(\gamma)}\pi_k^{(\gamma)}+\rho^{(\nu)}\pi_k^{(\nu)}. \tag{90}$$

2. Tensor mode

For tensor modes, we expand the first-order perturbation variables in the rank-2, zero-order PSTF tensor eigenfunctions $Q_{ab}^{(k)}$ of the comoving Laplacian,

$$S^2D^cD_cQ_{ab}^{(k)}=k^2Q_{ab}^{(k)}. \tag{91}$$

Similar to the case of scalar modes, this equation holds at the zero order. The tensor harmonics are transverse, orthogonal to u^a, and constant along the integral curves of u^a:

$$D^aQ_{ab}^{(k)}=0,\qquad u^aQ_{ab}^{(k)}=0,\qquad \dot{Q}_{ab}^{(k)}=0. \tag{92}$$

They can also be classified as having electric parity (denoted by $Q_{ab}^{(k)}$) or magnetic parity (denoted by $\bar{Q}_{ab}^{(k)}$). These two parity harmonics are related by a curl:

$$\text{curl}\ Q_{ab}^{(k)}=\frac{k}{S}\sqrt{1+\frac{3K}{k^2}}\bar{Q}_{ab}^{(k)}, \tag{93}$$

$$\text{curl}\ \bar{Q}_{ab}^{(k)}=\frac{k}{S}\sqrt{1+\frac{3K}{k^2}}Q_{ab}^{(k)}. \tag{94}$$

For tensor mode perturbations, the vorticity and all gauge-invariant vectors vanish at the first order; i.e. ω_{ab}, X_a, Z_a, q_a, A_a, $\mathcal{V}_a$, η_a all equal zero [45,52]. The rest of the rank-2 gauge-invariant tensors are constrained to be transverse:

$$^{(3)}\nabla^aE_{ab}=0,\qquad ^{(3)}\nabla^aB_{ab}=0,$$
$$^{(3)}\nabla^a\sigma_{ab}=0,\qquad ^{(3)}\nabla^a\pi_{ab}=0. \tag{95}$$

And they can be expanded in electric and magnetic parity tensor harmonics:

$$E_{ab}=\sum_k\frac{k^2}{S^2}(E_kQ_{ab}^{(k)}+\bar{E}_k\bar{Q}_{ab}^{(k)}), \tag{96}$$

$$B_{ab} = \sum_k \frac{k^2}{S^2}(B_k Q^{(k)}_{ab} + \bar{B}_k \bar{Q}^{(k)}_{ab}), \tag{97}$$

$$\sigma_{ab} = \sum_k \frac{k}{S}(\sigma_k Q^{(k)}_{ab} + \bar{\sigma}_k \bar{Q}^{(k)}_{ab}), \tag{98}$$

$$\pi^{(i)}_{ab} = \rho^{(i)} \sum_k (\pi^{(i)}_k Q^{(k)}_{ab} + \bar{\pi}^{(i)}_k \bar{Q}^{(k)}_{ab}). \tag{99}$$

Substituting these into the equations in Sec. III B, we obtain the E_k and σ_k propagation equations:

$$k^2 E_k' + k^2 E_k\left(\mathcal{H} + \frac{1}{2}\frac{\varphi'}{\varphi}\right) - k^3\left(1 + 3\frac{K}{k^2}\right)\sigma_k + \frac{\kappa S^2}{2\varphi}(\rho + P)k\sigma_k + \frac{\varphi'^2}{2\varphi^2}\left(\omega + \frac{3}{2}\right)k\sigma_k + \frac{\kappa S^2 \rho \pi_k}{\varphi}\mathcal{H} + \frac{3}{2}\frac{\kappa S^2 P \pi_k}{\varphi}\mathcal{H} + \frac{3}{4}\frac{\varphi'}{\varphi^2}\kappa S^2 \rho \pi_k - \frac{1}{2\varphi}\kappa S^2 \rho \pi_k' = 0, \tag{100}$$

$$\sigma_k' = -\mathcal{H}\sigma_k - kE_k - \frac{\kappa}{2k}\frac{S^2 \rho \pi_k}{\varphi} - \frac{1}{2}\frac{\varphi'}{\varphi}\sigma_k. \tag{101}$$

IV. NUMERICAL IMPLEMENTATION

We carry out our numerical study by modifying the CAMB code. The original CAMB code, written by Antony Lewis and Anthony Challinor [53], is a FORTRAN 90 program which calculates CMB anisotropies in the standard Einstein general relativity, by solving the Boltzmann-Einstein equations for various components in the Universe. Most of the equations to be solved are in the file *equations.f90*, which can be modified conveniently. The background evolution equation $d\tau/da$ is written in the function *dtauda*, and it can be modified for different backgrounds. The Boltzmann-Einstein equation group is listed in the functions *fderivs* (scalar mode for the flat universe), *fderivst* (tensor mode for the flat universe), *derivs* (scalar mode for the nonflat universe) and *derivst* (tensor mode for the nonflat universe). This equation group includes the propagation equations of the scalar factor S, the three-Ricci scalar perturbation η, the cold dark matter perturbation X_c, the baryon perturbations X_b and v_b, photon multipole moments, and neutrino multipole moments in the covariant approach. The CAMB code uses the Runge-Kutta method (subroutine dverk in file subroutines.f90) to solve these equations. To speed up the calculation, the line-of-sight integration method first developed by Seljak and Zaldarriaga [54] is used: the differential equation for the photon temperature perturbation is integrated along the line of sight to obtain $\delta T/T$. The multipoles today are definite integrals of the source term multiplied by the spherical Bessel functions from early times to today. The source term of the scalar perturbation at a given time for a given wave number is encoded in the subroutine *output*. The subroutine evolves the perturbation equations and does the integration in the cmbmain.f90 file. The main routine for running CAMB is wrapped in the file camb.f90. Using these equations, we modify the code for calculation in Brans-Dicke theory. The three most important parts of the modifications are the background evolution, the Boltzmann-Einstein differential equations, and the source term in the line-of-sight integration.

For the background evolution, we implement the procedure described in the Appendix of Ref. [14]. To satisfy the end point condition Eq. (10), we start from an epoch which is deemed early enough. We then evolve the model forwards (to avoid numerical instability, we do not evolve backwards) to obtain the φ value today. The procedure is repeated with a Brent algorithm (see e.g. [55]) to find the initial value of φ at that epoch. In doing this we set $\varphi' = 0$ and $\mathcal{V}_k = \mathcal{V}_k' = 0$ at the initial point. The initial condition $\varphi' = 0$ can be justified by Eq. (8): in the radiation dominated era, the right-hand side of Eq. (8), $\rho - 3P$, is negligible compared with other terms. Then

$$\varphi' = c_1 + c_2 S^{-2}. \tag{102}$$

This mean that any initial velocity quickly dies out in a few Hubble times and approaches a terminal velocity c_1; this velocity is constrained by nucleosynthesis, so it should be very small. The initial condition $\mathcal{V}_k = \mathcal{V}_k' = 0$ is the simplest choice which matches the requirement of Eq. (87). Initial perturbations in φ are damped during the radiation dominated era, so the choice of the initial condition of $\mathcal{V}_k$ has little impact on CMB anisotropy in the adiabatic perturbation case.

To realize the background evolution described above, we write a separate module. The function of this module is that, for a given value of φ today which is determined by the Brans-Dicke parameter ω, we first find out the initial value of φ at a sufficiently early time which can evolve the given value of φ today. Then we could calculate φ and φ' at each scale factor S and store them into arrays for interpolation in subsequent processes. Therefore, if one wants to use φ and φ' in the code, one must simply use this module first.

To be consistent with modified Friedmann equation (7), in the code we define the critical density as

$$\rho_{cr} = \frac{3\varphi_0}{\kappa}H_0^2, \tag{103}$$

where H_0 is the Hubble parameter today and φ_0 is given in Eq. (10). This definition differs from the conventional one by an additional factor φ. The definition of the fractional density is the same as the traditional one: $\Omega^{(i)} = \rho_0^{(i)}/\rho_{cr}$. Because φ' approximately vanishes today (cf. Fig. 2), from Eq. (7) we find $\Omega_{\rm total} \simeq 1$ for the flat geometry. This definition is convenient in studying the nonflat universe. We also should note that the difference from the traditional

one is very small, in most case, less than 1%, because $\varphi_0 = 1.001$ when $\omega = 50$.

In this work we adopt the cosmological constant as dark energy; this is equivalent to setting the potential of the Brans-Dicke field to a constant. The more general case of extended quintessence [56–62] will be dealt with in future studies. Below, we adopt the ΛCDM model with Einstein gravity, which best fits the Wilkinson Microwave Anisotropy Probe five-year data [63], as our fiducial model, i.e. $\Omega_b h^2 = 0.022\,65$, $\Omega_c h^2 = 0.1143$, $H_0 = 70.1\ \mathrm{km\,s^{-1}\,Mpc^{-1}}$, $n_s = 0.960$, $\Delta^2_{\mathcal{R}} = 2.457 \times 10^{-9}$ at $k = 0.002\ \mathrm{Mpc}^{-1}$, $\tau = 0.084$, and the dark energy equation of state, $w = -1$.

For the Boltzmann-Einstein differential equations, we modified the scale factor evolution equation and η_k propagation equation according to Eqs. (7) and (83), respectively, in the functions *fderivs* and *fderivst* in *equations. f90.* Some other complementary equations, such as the constraint equations, have also been modified correspondingly.

To speed up the calculation, the CAMB code integrates the system of differential equations by using the line-of-sight integration method, first developed by Seljak and Zaldarriaga for the CMBFAST code [54]. In this method, the multipole moment of photon intensity $I_k^{(l)}$ could be express as [41,64]

$$I_k^{(l)} = 4\int^{\eta_0} \mathrm{d}\eta S e^{-\tau}\Big\{\Big(\frac{k}{S}\sigma_k + \frac{1}{4}n_e\sigma_{\mathrm{T}}\kappa_2^{-1}\Big(\frac{3}{4}I_k^{(2)} + \frac{9}{2}\mathcal{E}_k^{(2)}\Big)\Big) \times \Big[\frac{1}{3}\Phi_l^\nu(x) + \frac{1}{k^2r^2}\frac{\mathrm{d}^2}{\mathrm{d}x^2}\Phi_l^\nu(x)\Big] + \sigma_{\mathrm{T}}v_k\frac{1}{kr}\frac{\mathrm{d}}{\mathrm{d}x}\Phi_l^\nu(x) - \Big[\frac{1}{3}\frac{k}{S}\mathcal{Z}_k - \frac{1}{4}n_e\sigma_{\mathrm{T}}I_k^{(0)}\Big]\Phi_l^\nu(x)\Big\}, \quad (104)$$

where η_0 is the conformal time today, $x = (\eta_0 - \eta)/r$, $r = 1/\sqrt{|K|}$, and τ is the zero-order optical depth back to x. Here,

$$\Phi_l^\nu(x) = \frac{l!}{(l-\nu)!}\frac{j_l(x)}{x^\nu} \quad (105)$$

are the ultraspherical Bessel functions, $\kappa_2 = (1 - 3K/k^2)^{1/2}$, and $\mathcal{E}_k^{(2)}$ is the quadrupole of the E-like polarization of the CMB photons. After integration by parts, one could eliminate the derivatives of ultraspherical Bessel functions and write temperature anisotropies as a time integral over a geometrical term $\Phi_l^\nu(x)$ and a source term:

$$I_k^{(l)} = 4\int^{\eta_0} \mathrm{d}\eta\Phi_l^0(x) \times \mathcal{S}, \quad (106)$$

where the source term is given by

$$\mathcal{S} = \frac{1}{12k^2\kappa_2}[12k\sigma_k''e^{-\tau}\kappa_2 + 24k\sigma_k'g(\eta)\kappa_2 + 12k\sigma_k g'(\eta)\kappa_2 + 3g''(\eta)\zeta_k + 6g'(\eta)\zeta_k' + 3g(\eta)\zeta_k'' + 12k\kappa_2 g'(\eta)v_k + 12k\kappa_2 g(\eta)v_k' + 4k^3\sigma_k e^{-\tau}\kappa_2 + k^2 g(\eta)\zeta_k - 4k^3e^{-\tau}\mathcal{Z}_k\kappa_2 + 3k^2 g(\eta)I_k^{(0)}\kappa_2], \quad (107)$$

in which

$$\zeta_k = \tfrac{3}{4}I_k^{(2)} + \tfrac{9}{2}\mathcal{E}_k^{(2)}, \quad (108)$$

$$g(\eta) = -\tau' e^{-\tau} = n_e\sigma_{\mathrm{T}}Se^{-\tau}, \quad (109)$$

where $g(\eta)$ is the visibility function. Using the first-order derivative perturbation equations described in Sec. III, σ_k'' and ζ_k'' in the source terms could be further expanded to the zeroth- and first-order derivative terms which are expressed in variables used in the *output* subroutine in the CAMB code.

V. RESULTS

In Fig. 1, we show the time evolution of the Brans-Dicke field φ. For models with $\omega > 0$, the value of φ increases with time, whereas for models with $\omega < 0$, φ decreases with time. During the radiation dominated era, the variation of φ is very small, almost zero. When entering the matter dominated epoch, φ begins to increase or decrease. After the domination of the dark energy, φ changes more rapidly. We also plot the time evolution of φ' in Fig. 2; as can be seen from that figure, $|\varphi'|$ reaches a terminal velocity in the radiation dominated era, and then begins to decay in the matter dominated epoch, but as the dark energy becomes dominant, it increases again, and its present-day value for this particular model is of the order 10^{-6}.

The effective Newtonian gravitational coupling G_{eff} is the inverse of φ in units of G. The time evolutions of G_{eff} are shown in Fig. 3. We can see that G_{eff} changes rapidly at

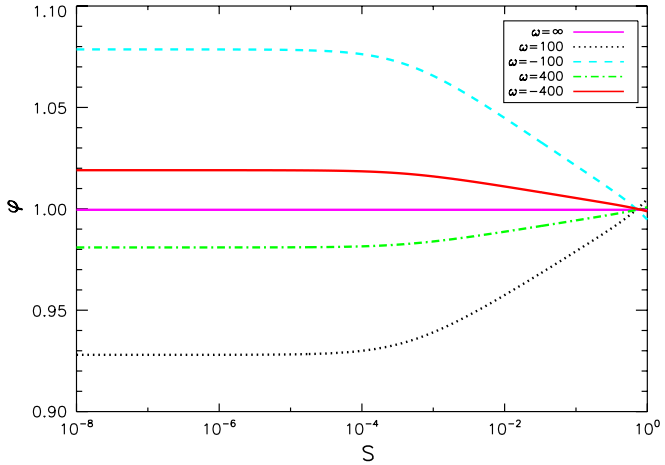

FIG. 1 (color online). The time evolution of the Brans-Dicke field φ.

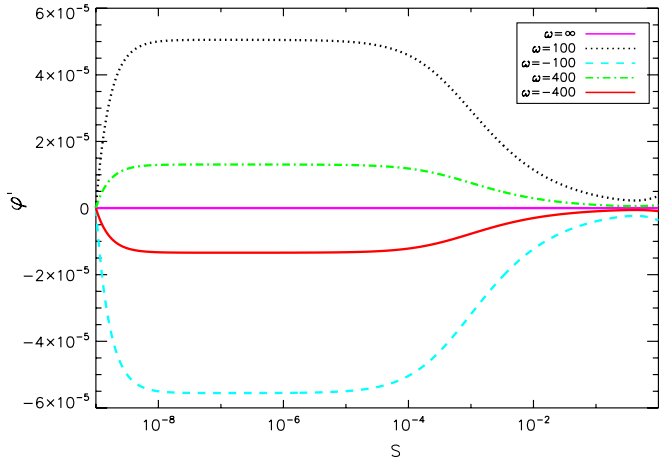

FIG. 2 (color online). The evolution of the time derivative of the Brans-Dicke field φ'.

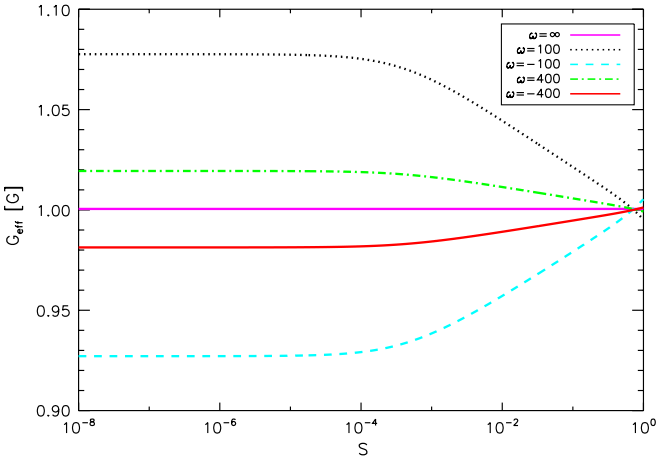

FIG. 3 (color online). The time evolution of the effective Newtonian gravitational coupling $G_{\rm eff}$.

low redshift, so it may not be reliable to use the type Ia supernovae (SNe Ia) data to constrain Brans-Dicke theory: the Chandrasekhar mass $M_{\rm Ch} \propto G^{-3/2}$, so the variation of the gravitational coupling G means that the peak luminosity of SNe, which is approximately proportional to the Chandrasekhar mass, may also change, making it unreliable as a standard candle.

The CMB angular power spectra for the Brans-Dicke theory with $\omega = \infty$ (i.e. general relativity) and ± 75 are plotted in Fig. 4, and the resulting differences are plotted in Fig. 5. As can be seen, compared with the general relativity theory with the same cosmological parameters, both the location and the height of the CMB acoustic peaks are changed. The Brans-Dicke model with a positive ω has broader and lower acoustic peaks for this set of parameters. As $|\omega|$ increases, the difference in CMB angular spectra between Brans-Dicke theory and general relativity diminishes. The difference is more apparent at large l (small angular scale), so high resolution CMB data would be very useful in distinguishing the different models. From Fig. 4, it is also very clear that the polarization spectra have a strong discriminating power. With the higher angular resolution and polarization data that we expect in the near future, we should be able to lift the degeneracy of parameters and place a more stringent constraint on the Brans-Dicke models.

We compare the result of our new code with those obtained with the CMBFAST code in the synchronous gauge[1] in Ref. [14]. We find that the difference in the CMB power spectra is typically less than 1% and is due primarily to the difference in the original (Einstein gravity) codes—for really making highly precise constraints on cosmological parameters with the CMB data, the precision of the CMB Boltzmann code needs to be further improved. The new code of course has better program architecture and runs faster. Particularly, if one calculates $\partial C_l/\partial\omega$, which reflects the impact of the gravity model on the CMB angular power spectrum, the results of the two codes agree with each other at high precision, as shown in Fig. 5. The result on $\Delta C_l = C_l(\omega = \infty) - C_l(\omega = 75)$ for TT, TE, and EE correlations are very consistent in the two codes, and the two curves are almost indiscernible in Fig. 5.

We also plot the CMB temperature and polarization spectra yielded by tensor modes in Fig. 6.

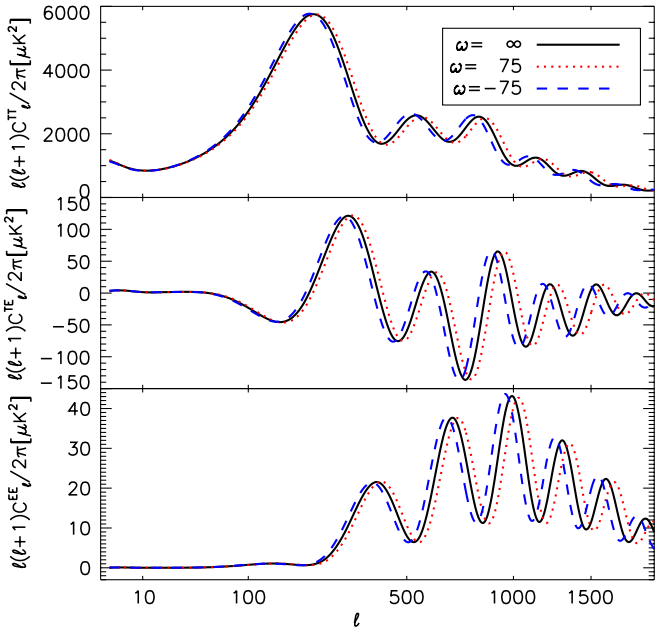

FIG. 4 (color online). CMB temperature and polarization power spectra for Brans-Dicke theories with $\omega = \infty$, ± 75 in the scalar mode.

[1]There are some typos in Eqs. (19) and (20) of Ref. [14]. A prime $'$ was missed in the last term of Eq. (19); i.e. it should read $\frac{3a'\chi'}{a\phi}$. A factor of 2 in the denominator was missed in the last term of Eq. (20); i.e., it should read $\frac{-1}{2\phi}(\chi' - \frac{a'\chi}{a})$. Most conclusions of that paper were not affected, but at small ℓ the C_ℓ was slightly overestimated.

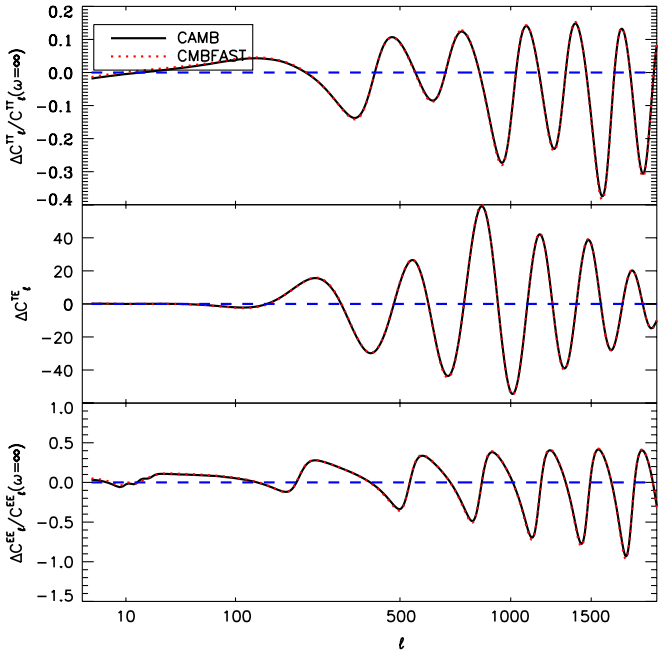

FIG. 5 (color online). $\Delta C_l = C_l(\omega = \infty) - C_l(\omega = 75)$ for TT, TE, and EE correlations.

The tensor-to-scalar ratio is set to 0.1. The primordial gravitational wave produces large temperature fluctuations at large scales, as well as a unique B mode polarization. In contrast to scalar modes, when compared with the result of general relativity, the peaks are higher for positive ω. Similar to the scalar mode, positive ω shifts the peaks to smaller scales. At both the very large scales and very small scales, the differences in spectra between Brans-Dicke theory and general relativity are very small, almost invisible, and the differences are only sensitive at $l \sim 80$.

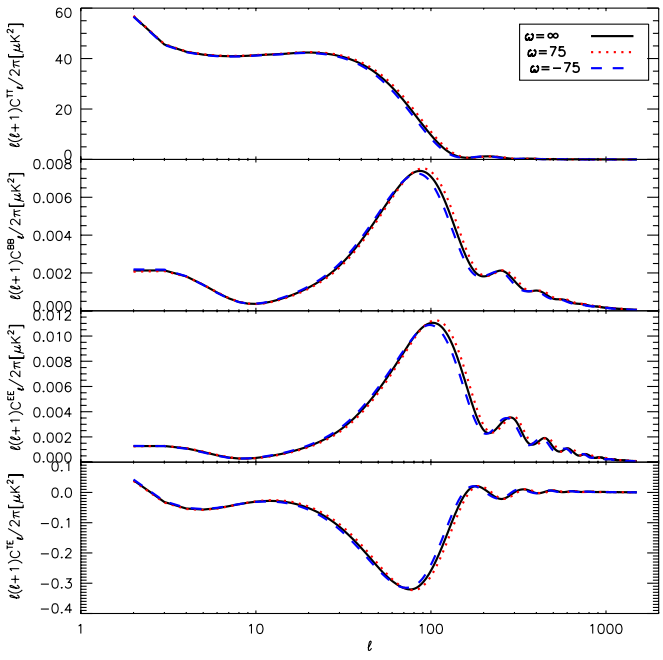

FIG. 6 (color online). CMB temperature and polarization power spectra for the Brans-Dicke theories in the tensor mode. The solid, dotted, and dashed curves represent the Brans-Dicke model with $\omega = \infty$, 75, and -75, respectively. The tensor-to-scalar ratio R is set to 0.1.

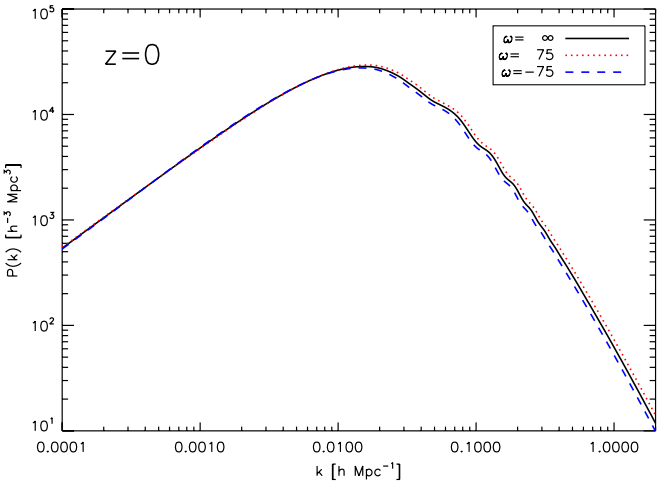

FIG. 7 (color online). The matter power spectra at $z = 0$. The solid, dotted, and dashed curves represent the Brans-Dicke model with $\omega = \infty$, 75, and -75, respectively.

Figure 7 shows the impact of the Brans-Dicke field on the matter power spectra at $z = 0$. For $\omega = 75$, the bend of the matter power spectrum occurs at short wavelengths, and there is thus more small scale power, in agreement with the prediction of Ref. [65].

VI. INTEGRATED SACHS-WOLFE EFFECT AND GRAVITATIONAL LENSING

The ISW effect is the secondary CMB anisotropy caused by the time-varying gravitational potential Φ. The CMB temperature fluctuation of the ISW effect in the direction $\hat{\mathbf{n}}$ is given by

$$\delta_T^{\mathrm{ISW}}(\hat{\mathbf{n}}) \equiv \frac{\Delta_T^{\mathrm{ISW}}(\hat{\mathbf{n}})}{T_0} = -2\int_0^{z_{\mathrm{LS}}} dz \frac{\partial \Phi}{\partial z}(\hat{\mathbf{n}}, z), \qquad (110)$$

where $T_0 = 2.725$ K is the CMB temperature at the present time, and z_{LS} is the redshift at the surface of last scattering. Despite its small size, the ISW effect provides an independent test of dark energy, and as the effect is produced by a change in the gravitational potential, it could potentially be a new probe of modified gravity. We examine its impact on two observables: the CMB temperature anisotropy autocorrelation power spectrum, and the cross correlation between CMB anisotropy and the galaxy overdensity along the line of sight.

First we look at the CMB TT correlation. The C_l^{ISW} spectra shown in Fig. 8 are the temperature anisotropy power spectra produced by the ISW effect; i.e. these are calculated by including only the $\dot{\Psi}$ and $\dot{\Phi}$ (Newtonian gauge

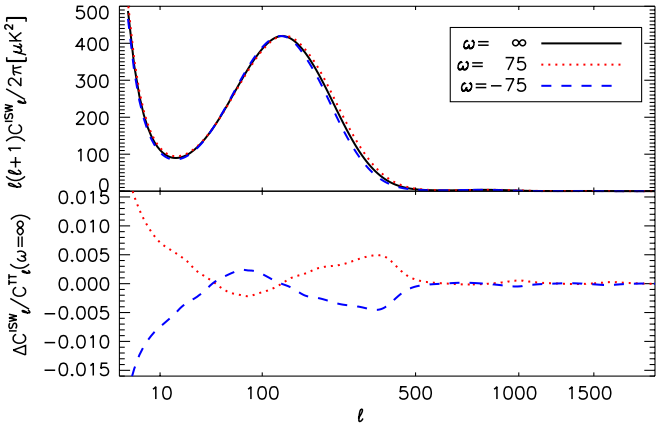

FIG. 8 (color online). The ISW effect of the TT power spectra in the scalar mode for Brans-Dicke gravity. $C_l^{\rm ISW}$ is the CMB TT power spectrum only considering the ISW effect. $\Delta C_l^{\rm ISW} = C_l^{\rm ISW}(\omega') - C_l^{\rm ISW}(\omega = \infty)$, $\omega' = 75$ for the red dotted curve, and $\omega' = -75$ for the blue dashed curve.

variables) terms in the line-of-sight integration with different models. According to the time when it occurred, the ISW effect can usually be divided into two types: the early ISW effect during the radiation dominated to matter dominated transition, and the late ISW effect during the matter dominated to dark energy dominated transition. The peaks of their contribution to the angular power spectrum have positions corresponding to the respective horizon sizes. Thus, the early ISW effect produces the peak at $l \sim 150$, while the late ISW effect produces the slope at small l.

In the bottom panel of Fig. 8, we plot $\Delta C_l^{\rm ISW}/C_l^{\rm TT}(\omega = \infty)$, i.e. the ratio of the ISW modification in Brans-Dicke gravity to the total TT power spectrum of CMB in GR, where $\Delta C_l^{\rm ISW} \equiv C_l^{\rm ISW}(\omega = 75) - C_l^{\rm ISW}(\omega = \infty)$ is plotted with the red dotted curve, while $\omega = -75$ is plotted with the blue dashed curve. Here $C_l^{\rm TT}(\omega = \infty)$ is the TT power spectrum including all effects with $\omega = \infty$ (the GR case). The correction of the late ISW effect (at the lowest l) caused by Brans-Dicke theory is of the order of 1% of the total TT power spectrum, and the correction from the early ISW effect (at $l \sim 150$) is only about half of that size. This correction is buried in the cosmic variance, and it would be hard to distinguish Brans-Dicke gravity from general relativity with this effect.

The cross correlation between CMB temperature and galaxy overdensity along the line of sight can also be used to measure the ISW effect. To calculate this effect, we consider the observed galaxy density contrast in the direction $\hat{\mathbf{n}}$,

$$\delta_g(\hat{\mathbf{n}}) = \int b_g(z)\frac{dN}{dz}(z)\delta_m(\hat{\mathbf{n}}, z)dz. \tag{111}$$

We assume that the bias is a constant, $b_g(z) = 1.3$. The selection function dN/dz describes the redshift distribution of the galaxy sample; here we adopt the analytic function from Ref. [66]:

$$\frac{dN}{dz} \propto z^2 e^{-(z/z')^{3/2}}, \tag{112}$$

where $z' = z_m/1.412$. z_m is the median redshift of the survey, which we set as $z_m = 0.33$, and this galaxy redshift distribution is shown in Fig. 9, with the normalization of the distribution satisfying $\int dN/dz = 1$. The gravitational potential Φ is related to the matter density fluctuation δ via the Poisson equation:

$$\nabla^2\Phi(\hat{\mathbf{n}}, z) = 4\pi G a^2 \rho_{\rm m}(z)\delta(\hat{\mathbf{n}}, z) \tag{113}$$

or

$$\Phi(\mathbf{k}, z) = -\frac{3}{2}\Omega_{\rm m}\left(\frac{H_0}{ck}\right)^2\frac{\delta(\mathbf{k}, z)}{a}, \tag{114}$$

where $\rho_{\rm m} = \rho_{\rm m}^0 a^{-3}$.

The angular cross correlation of the CMB temperature and galaxy fluctuation is given by

$$w_{gT}^{\rm ISW}(\theta) \equiv \langle\delta_g(\hat{\mathbf{n}}_1)\Delta_T(\hat{\mathbf{n}}_2)\rangle \tag{115}$$

$$= \langle\delta_g(\hat{\mathbf{n}}_1)\Delta_T^{\rm ISW}(\hat{\mathbf{n}}_2)\rangle, \tag{116}$$

where $\hat{\mathbf{n}}_1 \cdot \hat{\mathbf{n}}_2 = \cos\theta$. Note that $\Delta_T(\hat{\mathbf{n}})$ is the total temperature fluctuation in a given direction $\hat{\mathbf{n}}$, while $\Delta_T^{\rm ISW}(\hat{\mathbf{n}})$ is the temperature fluctuation caused only by the ISW effect [see Eq. (110)]; the identities hold because the CMB temperature fluctuations caused by other effects do not correlate with galaxy overdensity. Expand $\delta_m(\hat{\mathbf{n}}, z)$ in Eq. (111) into Fourier modes:

$$\delta_{\rm m}(\hat{\mathbf{n}}, z(\chi)) = \delta_{\rm m}(\hat{\mathbf{n}}\chi, z) \tag{117}$$

$$= \int\frac{d^3k}{(2\pi)^3}\delta_{\rm m}(k, z)e^{-i\mathbf{k}\cdot\hat{\mathbf{n}}\chi}, \tag{118}$$

where χ is the comoving distance from redshift 0 to z; then further expand $e^{-i\mathbf{k}\cdot\hat{\mathbf{n}}\chi}$ as

$$e^{-i\mathbf{k}\cdot\hat{\mathbf{n}}\chi} = 4\pi\sum_{lm}(-i)^l j_l(k\chi)Y_{lm}(\hat{\mathbf{n}})Y_{lm}^*(\hat{\mathbf{k}}), \tag{119}$$

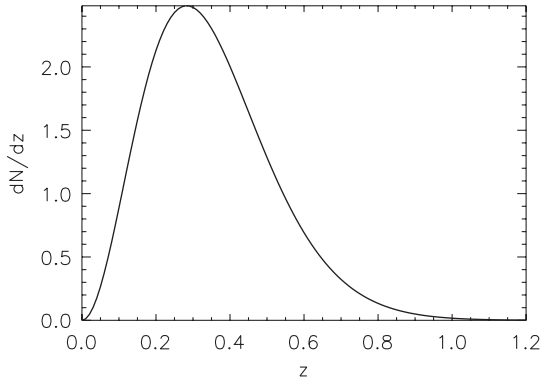

FIG. 9. The redshift distribution of the assumed sample with median redshift $z_m = 0.33$.

where $j_l(x)$ is the spherical Bessel function of the first kind of rank l and $Y_{lm}(\hat{\mathbf{k}})$ is the spherical harmonic function. Substituting Eqs. (118) and (119) into Eq. (111), we obtain

$$\delta_g(\hat{\mathbf{n}}) = \sum_{lm} \delta_{g,lm} Y_{lm}(\hat{\mathbf{n}}), \tag{120}$$

where

$$\delta_{g,lm} = (-i)^l \int \frac{d^3k}{(2\pi)^3} \int dz 4\pi j_l(k\chi) Y^*_{lm}(\hat{\mathbf{k}}) b_g(z) \times \frac{dN}{dz}(z)\delta(\mathbf{k}, z). \tag{121}$$

Similarly,

$$\Delta^{\mathrm{ISW}}_T(\hat{\mathbf{n}}) = \sum_{lm} \Delta^{\mathrm{ISW}}_{T,lm} Y_{lm}(\hat{\mathbf{n}}), \tag{122}$$

where

$$\Delta^{\mathrm{ISW}}_{T,lm} = (-i)^l \int \frac{d^3k}{(2\pi)^3} \int dz 4\pi j_l(k\chi(z)) Y^*_{lm}(\hat{\mathbf{k}}) 3\Omega_{\mathrm{m}} T_0 \times \left(\frac{H_0}{kc}\right)^2 \frac{\partial}{\partial z}\left[\frac{\delta(\mathbf{k}, z)}{a(z)}\right]. \tag{123}$$

The angular cross-correlation power spectrum of the galaxy overdensity and ISW temperature perturbation is then

$$C^{\mathrm{ISW}}_{gT}(l) \equiv \delta_{ll'}\delta_{mm'}\langle \delta_{g,lm}\Delta^*_{T,l'm'}\rangle. \tag{124}$$

Using the small angle (large l, $l \gg 1$) approximation for the spherical Bessel functions [67],

$$j_l(x) = \sqrt{\frac{\pi}{2l+1}}\left[\delta_{\mathrm{Dirac}}\left(l + \frac{1}{2} - x\right) + \mathbf{O}(l^{-2})\right], \tag{125}$$

we have [68]

$$\frac{2}{\pi}\int k^2 dk j_l(k\chi) j_l(k\chi') = \frac{1}{\chi^2}\delta(\chi - \chi'). \tag{126}$$

Another useful relation will be the definition of $D(z)$: $\delta(\mathbf{k}, z) = D(z)\delta(\mathbf{k}, 0)$. Under the Limber approximation [69,70], we have

$$C^{\mathrm{ISW}}_{gT}(l) = \frac{4}{(2l+1)^2}\int dz P(k) W_{\mathrm{ISW}}(z) W_g(z) \frac{H(z)}{c}, \tag{127}$$

where $P(k)$ is the linear power spectrum at redshift zero, $k \approx (l + 1/2)/\chi(z)$ obtained from Eq. (125), and $W_{\mathrm{ISW}}(z)$ and $W_g(z)$ are the ISW and galaxy window functions defined as

$$W_{\mathrm{ISW}}(z) \equiv 3\Omega_{\mathrm{m}} T_0 \left(\frac{H_0}{c}\right)^2 \frac{d}{dz}\left[\frac{D(z)}{a(z)}\right] \tag{128}$$

and

$$W_g(z) \equiv b_g(z)\frac{dN}{dz}(z)D(z). \tag{129}$$

Finally, $w^{\mathrm{ISW}}_{gT}(\theta)$ is related to the cross-power spectrum by the Legendre polynomials,

$$w^{\mathrm{ISW}}_{gT}(\theta) = \sum_{l=2}^{\infty} \frac{2l+1}{4\pi} P_l(\cos\theta) C^{\mathrm{ISW}}_{gT}(l). \tag{130}$$

This summation does not include the monopole ($l = 0$) and dipole ($l = 1$) terms, as in the Wilkinson Microwave Anisotropy Probe analysis [71].

We plot the result in Fig. 10. The upper panel shows the angular power spectrum, while the bottom panel is the angular correlation function. For the angular power spectra, Brans-Dicke theory with $\omega = \pm 75$ differs from the GR case by about 3%–8% on large scales ($l < 14$); for the angular correlation function, there is a difference of 3%–4% for $\theta <$ 100 arcmin, and on larger angles ($\theta > 100$ arcmin) the difference is even larger. At present the CMB-galaxy correlation data could merely confirm the ISW effect up to about the 3σ level, and the data are often plagued by systematic errors which are not well understood yet, as the observational results are often in conflict with each other [68,71–73]. Recently, it has been noted that for models in which the gravitational constant has drastic changes at low redshift, the ISW effect could be significant and thus provide a sensitive probe of modified gravity [74–76]. However, for the models discussed here, the variation of the gravitational potential at low redshift is actually not that large; thus, including the ISW effect does not yield any significant difference.

How is the weak gravitational lensing effect modified in Brans-Dicke theory? We investigate this problem by modifying the CAMB code to include the lensing effect for

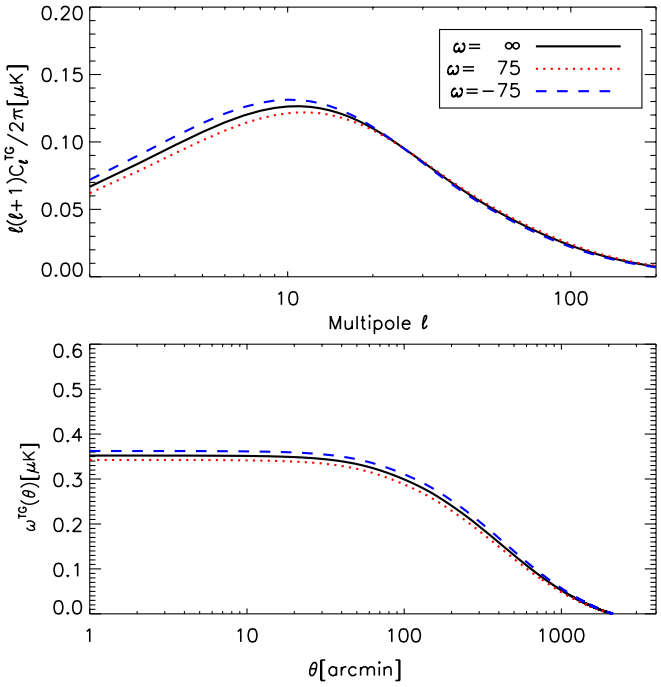

FIG. 10 (color online). The ISW effect from the CMB temperature and galaxy overdensity correlation. The upper panel is the angular power spectrum, while the bottom panel is the angular correlation function.

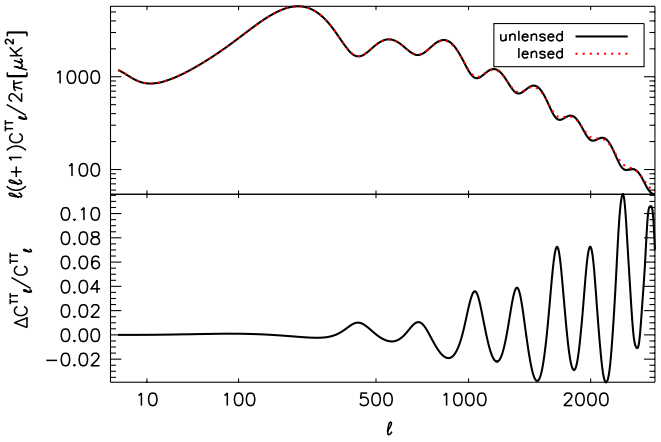

FIG. 11 (color online). Comparison of unlensed and lensed CMB TT power spectra in the scalar mode for Brans-Dicke gravity with $\omega = 75$. $\Delta C_l^{\mathrm{TT}}/C_l^{\mathrm{TT}}$ is the relative difference, where $\Delta C_l^{\mathrm{TT}} = C_l^{\mathrm{TT}}(\mathrm{lensed}) - C_l^{\mathrm{TT}}(\mathrm{unlensed})$, and C^{TT} in the denominator is the unlensed TT power spectrum.

Brans-Dicke theory. The CMB lensing effect in Brans-Dicke gravity is similar to that in general relativity; it smooths the CMB power spectra at small scales. The result is shown in Fig. 11, for $\omega = 75$. At $l > 500$, we begin to see corrections due to Brans-Dicke theory at the percent level, so in the future when the Planck data become available, this effect should be included in the calculation. At $l > 2000$, the correction could reach as high as the 10% level, but there the CMB primordial anisotropy is strongly damped and the anisotropy is dominated by the Sunyaev-Zel'dovich effect.

VII. CONCLUSION AND SUMMARY

Compared with Einstein's general relativity, there is an additional scalar field coupled with the Ricci scalar in Brans-Dicke gravity, which makes the perturbation theory more complicated. With a covariant $1 + 3$ approach, we have developed a full set of covariant and gauge-invariant formalism for calculating the cosmic microwave background temperature and polarization anisotropies in Brans-Dicke gravity. Instead of using the components of the metric as basic variables, the covariant formalism performs a $1 + 3$ split of the Bianchi and Ricci identities, using the kinematic quantities, energy-momentum tensors of the fluid(s), and the gravito- electromagnetic parts of the Weyl tensor to study how perturbations evolve. Adopting covariantly defined, gauge-invariant variables throughout ensures that, in our discussion, the gauge ambiguities are avoided and that all variables have a clear, physical interpretation. Since the definition of the covariant variables does not assume any linearization, exact equations can be found for their evolution, which can then be linearized around the chosen background model. Furthermore, unified treatment of scalar, vector, and tensor modes does not require decomposing the different modes from the beginning as done in the metric method. The price we have to pay is that with this method the calculation is more complicated.

We then calculate the CMB temperature and polarization spectra for the Brans-Dicke models using a modified CAMB code. In this paper we consider both the scalar modes and the tensor modes as the adiabatic initial condition, and adopt $\varphi_0 = (2\omega + 4)/(2\omega + 3)$ at the current epoch and $\varphi' = 0$ at early times as initial conditions of the Brans-Dicke field. Compared with the general-relativistic model with the same cosmological parameters, both the amplitude and the width of the acoustic peaks are different in the Brans-Dicke models. We find that the small scale spectra and the polarization spectra will provide a sensitive and vigorous constraint on the different Brans-Dicke models in the scalar mode. For tensor modes, the largest difference in CMB spectra for various Brans-Dicke models is located at $l \sim 80$. The structure formation process in Brans-Dicke theory is also studied. The matter power spectrum is shown in Fig. 7. For the positive ω case, the bend of the matter power spectra occurs at shorter wavelengths, and there is thus more small scale power compared with the general relativity case.

The ISW effect of Brans-Dicke theory is investigated (see Figs. 8 and 10). The corrections to the total TT power spectra that come from the early ISW effect caused by Brans-Dicke theory are proved to be of the order of 1%, and the late ISW effect is only half of the early ISW effect. Because of the large cosmic variance at large scales, this effect is not significant in the observational constraint. For CMB-galaxy cross correlation, the differences between the GR case and the Brans-Dicke case with $\omega = \pm 75$ are at the 3%–8% level on large scales ($l < 14$) in angular power spectra, or 3%–4% in the angular correlation function for $\theta < 100$ arcmin; on even larger angular scales ($\theta > 100$ arcmin) the difference is still larger. Nevertheless, for the modified gravity model considered here, where the variation in the gravitational potential at low redshift is not very large, the ISW effect does not provide a very sensitive probe due to the large cosmic covariances.

The CMB lensing effect is plotted in Fig. 11. This effect only appears significantly at $l > 2000$. The lensed CMB power spectra look smooth at small scales compared with the unlensed power spectra in Brans-Dicke gravity, which is very similar to the case of general relativity.

Our covariant calculation for the Brans-Dicke model is generally in agreement with the previous results obtained in particular gauges (e.g. the synchronous gauge [14]). Furthermore, we have also obtained for the first time the temperature and polarization spectra for tensor mode perturbations, the ISW effect, and the CMB lensing effect in Brans-Dicke theory. The structure and speed of the code are greatly improved, thus providing a more powerful and convenient tool for further studies. In paper II, we use the Markov-Chain Monte Carlo algorithm to derive the constraint on the Brans-Dicke parameter ω with the latest CMB and large scale structure observational data.

As a final remark, the covariant approach and corresponding CMB code for the Brans-Dicke theory developed in this paper, together with the synchronous gauge approach and the corresponding code developed in the previous paper [14], provide consistent, systematic, and complete methods to study Brans-Dicke theory. These methods and codes could be generalized to study more general scalar-tensor theories, as well as more complex initial conditions; we plan to carry out such a generalization in subsequent studies.

ACKNOWLEDGMENTS

We thank Antony Lewis, G. F. R. Ellis, Marc Kamionkowski, and Gong-Bo Zhao for helpful discussions. Our Markov-Chain Monte Carlo computation was performed at the Supercomputing Center of the Chinese Academy of Sciences and the Shanghai Supercomputing Center. X. C. acknowledges the hospitality of the Moore Center of Theoretical Cosmology and Physics at Caltech, where part of this research was performed. This work is supported by the National Science Foundation of China under Grant No. 10525314 and the Key Project Grant No. 10533010; by the Chinese Academy of Sciences under Grant No. KJCX3-SYW-N2; by the Ministry of Science and Technology under the National Basic Science Program (Project 973) Grant No. 2007CB815401; and by the Young Researcher Grant of National Astronomical Observatories, Chinese Academy of Sciences.

[1] P. Jordan, Nature (London) **164**, 637 (1949).
[2] P. Jordan, Z. Phys. **157**, 112 (1959).
[3] M. Fierz, Helv. Phys. Acta **29**, 128 (1956).
[4] C. Brans and R. H. Dicke, Phys. Rev. **124**, 925 (1961).
[5] R. H. Dicke, Phys. Rev. **125**, 2163 (1962).
[6] P. G. Bergmann, Int. J. Theor. Phys. **1**, 25 (1968).
[7] K. Nordtvedt, Jr., Astrophys. J. **161**, 1059 (1970).
[8] R. V. Wagoner, Phys. Rev. D **1**, 3209 (1970).
[9] J. D. Bekenstein, Phys. Rev. D **15**, 1458 (1977).
[10] J. D. Bekenstein and A. Meisels, Phys. Rev. D **18**, 4378 (1978).
[11] P. J. E. Peebles and J. T. Yu, Astrophys. J. **162**, 815 (1970).
[12] H. Nariai, Prog. Theor. Phys. **42**, 742 (1969).
[13] J. P. Baptista, J. C. Fabris, and S. V. B. Goncalves, arXiv: gr-qc/9603015.
[14] X. Chen and M. Kamionkowski, Phys. Rev. D **60**, 104036 (1999).
[15] R. Nagata, T. Chiba, and N. Sugiyama, Phys. Rev. D **66**, 103510 (2002).
[16] J.-c. Hwang, Classical Quantum Gravity **14**, 1981 (1997).
[17] M. Lifshitz, J. Mosc. Phys. Soc. **10**, 116 (1946).
[18] J. M. Bardeen, Phys. Rev. D **22**, 1882 (1980).
[19] V. F. Mukhanov, H. A. Feldman, and R. H. Brandenberger, Phys. Rep. **215**, 203 (1992).
[20] G. F. R. Ellis and M. Bruni, Phys. Rev. D **40**, 1804 (1989).
[21] S. W. Hawking, Astrophys. J. **145**, 544 (1966).
[22] O. Heckmann and E. Schücking, Z. Astrophys. **38**, 95 (1955).
[23] A. Raychaudhuri, Z. Astrophys. **43**, 161 (1957).
[24] G. F. R. Ellis, M. Bruni, and J. Hwang, Phys. Rev. D **42**, 1035 (1990).
[25] G. F. R. Ellis and C. G. Tsagas, Phys. Rev. D **66**, 124015 (2002).
[26] G. F. R. Ellis and H. van Elst, NATO Adv. Study Inst. Ser. C, Math. Phys. Sci. **541**, 1 (1999).
[27] M. Bruni, P. K. S. Dunsby, and G. F. R. Ellis, Astrophys. J. **395**, 34 (1992).
[28] P. K. S. Dunsby, M. Bruni, and G. F. R. Ellis, Astrophys. J. **395**, 54 (1992).
[29] R. Maartens, Phys. Rev. D **55**, 463 (1997).
[30] R. Maartens and B. A. Bassett, Classical Quantum Gravity **15**, 705 (1998).
[31] R. Maartens, Phys. Rev. D **62**, 084023 (2000).
[32] C. G. Tsagas and J. D. Barrow, Classical Quantum Gravity **14**, 2539 (1997).
[33] C. G. Tsagas and R. Maartens, Classical Quantum Gravity **17**, 2215 (2000).
[34] C. G. Tsagas, Classical Quantum Gravity **22**, 393 (2005).
[35] C. G. Tsagas, A. Challinor, and R. Maartens, Phys. Rep. **465**, 61 (2008).
[36] B. Li and M. C. Chu, Phys. Rev. D **74**, 104010 (2006).
[37] B. Li, J. D. Barrow, and D. F. Mota, Phys. Rev. D **76**, 044027 (2007).
[38] B. Li, J. D. Barrow, and D. F. Mota, Phys. Rev. D **76**, 104047 (2007).
[39] H. van Elst and G. F. R. Ellis, Phys. Rev. D **59**, 024013 (1998).
[40] B. Leong, P. Dunsby, A. Challinor, and A. Lasenby, Phys. Rev. D **65**, 104012 (2002).
[41] A. Challinor, Phys. Rev. D **62**, 043004 (2000).
[42] A. Challinor, Classical Quantum Gravity **17**, 871 (2000).
[43] A. Challinor, Gen. Relativ. Gravit. **32**, 1059 (2000).
[44] R. Maartens, T. Gebbie, and G. F. R. Ellis, Phys. Rev. D **59**, 083506 (1999).
[45] A. Challinor and A. Lasenby, Phys. Rev. D **58**, 023001 (1998).
[46] A. Challinor and A. Lasenby, Astrophys. J. **513**, 1 (1999).
[47] T. Hirai and K.-i. Maeda, Astrophys. J. **431**, 6 (1994).
[48] S. Carloni, P. K. S. Dunsby, and C. Rubano, Phys. Rev. D **74**, 123513 (2006).
[49] S. Carloni and P. K. S. Dunsby, Phys. Rev. D **75**, 064012 (2007).
[50] F. Wu and X. Chen, following Article, Phys. Rev. D **82**, 083003 (2010)
[51] A. Lewis, A. Challinor, and A. Lasenby, Astrophys. J. **538**, 473 (2000).

[52] P. K. S. Dunsby, B. A. C. C. Bassett, and G. F. R. Ellis, Classical Quantum Gravity **14**, 1215 (1997).
[53] A. Lewis and A. Challinor, http://camb.info/ (1999).
[54] U. Seljak and M. Zaldarriaga, Astrophys. J. **469**, 437 (1996).
[55] W. H. Press, S. A. Teukolsky, W. T. Vetterling, and B. P. Flannery, *Numerical Recipes in Fortran: The Art of Scientific Computing* (Carmbige University Press, Cambridge, England, 1992), 2nd ed.
[56] J.-P. Uzan, Phys. Rev. D **59**, 123510 (1999).
[57] L. Amendola, Phys. Rev. D **60**, 043501 (1999).
[58] T. Chiba, Phys. Rev. D **60**, 083508 (1999).
[59] F. Perrotta, C. Baccigalupi, and S. Matarrese, Phys. Rev. D **61**, 023507 (1999).
[60] D. J. Holden and D. Wands, Phys. Rev. D **61**, 043506 (2000).
[61] C. Baccigalupi, S. Matarrese, and F. Perrotta, Phys. Rev. D **62**, 123510 (2000).
[62] X. Chen, R. J. Scherrer, and G. Steigman, Phys. Rev. D **63**, 123504 (2001).
[63] E. Komatsu *et al.* (WMAP Collaboration), Astrophys. J. Suppl. Ser.. **180**, 330 (2009).
[64] A. M. Lewis, Ph.D. thesis, University of Cambridge, 2000.
[65] A. R. Liddle, A. Mazumdar, and J. D. Barrow, Phys. Rev. D **58**, 027302 (1998).
[66] A. Cabré, P. Fosalba, E. Gaztañaga, and M. Manera, Mon. Not. R. Astron. Soc. **381**, 1347 (2007).
[67] N. Afshordi, Y.-S. Loh, and M. A. Strauss, Phys. Rev. D **69**, 083524 (2004).
[68] S. Ho, C. Hirata, N. Padmanabhan, U. Seljak, and N. Bahcall, Phys. Rev. D **78**, 043519 (2008).
[69] D. N. Limber, Astrophys. J. **117**, 134 (1953).
[70] M. LoVerde and N. Afshordi, Phys. Rev. D **78**, 123506 (2008).
[71] U. Sawangwit *et al.*, Mon. Not. R. Astron. Soc. **402**, 2228 (2010).
[72] M. Lopez-Corredoira, F. S. Labini, and J. Betancort-Rijo, Astron. Astrophys. **513**, A3 (2010).
[73] C. Hernandez-Monteagudo, arXiv:0909.4294.
[74] G.-B. Zhao *et al.*, Phys. Rev. D **81**, 103510 (2010).
[75] T. Giannantonio, M. Martinelli, A. Silvestri, and A. Melchiorri, J. Cosmol. Astropart. Phys. 04 (2010) 030.
[76] S. F. Daniel *et al.*, Phys. Rev. D **81**, 123508 (2010).